The magnetoelliptic instability of rotating systems

K. A. MIZERSKI[1,2]† AND K. BAJER[2]

[1]Department of Applied Mathematics, University of Leeds, Woodhouse Lane, Leeds LS2 9JT, UK

[2]Institute of Geophysics, University of Warsaw, Pasteura 7, 02-093 Warsaw, Poland

We address the question of stability of the Euler flow with elliptical streamlines in a rotating frame, interacting with uniform external magnetic field perpendicular to the plane of the flow. Our motivation for this study is of astrophysical nature, since many astrophysical objects, such as stars, planets and accretion discs, are tidally deformed through gravitational interaction with other bodies. Therefore, the ellipticity of the flow models the tidal deformations in the simplest way. The joint effect of the magnetic field and the Coriolis force is studied here numerically and analytically in the limit of small elliptical (tidal) deformations ($\zeta \ll 1$), using the analytical technique developed by Lebovitz & Zweibel (*Astrophys. J.*, vol. 609, 2004, pp. 301–312). We find that the effect of background rotation and external magnetic field is quite complex. Both factors are responsible for new destabilizing resonances as the vortex departs from axial symmetry ($\zeta \ll 1$); however, just like in the non-rotating case, there are three principal resonances causing instability in the leading order. The presence of the magnetic field is very likely to destabilize the system with respect to perturbations propagating in the direction of the magnetic field if the basic vorticity and the background rotation have opposite signs (i.e. for *anticyclonic* background rotation). We present the dependence of the growth rates of the modes on various parameters describing the system, such as the strength of the magnetic field (h), the inverse of the Rossby number ($\mathcal{R}_v$), the ellipticity of the basic flow (ϵ) and the direction of propagation of modes (ϑ). Our analytical predictions agree well with the numerical calculations.

1. Introduction

The *elliptical instability* is widely proposed as the so-called secondary instability in turbulence development. The experimental studies of the transition to turbulence (Cadot, Douady & Couder 1995; EloyLe Gal & Le Dizès 2000) as well as numerical simulations and theoretical arguments (Orszag & Patera 1983; Waleffe 1990; Le Dizes & Lacaze 2005) suggest that a three-dimensional instability develops in regions with closed elliptical streamlines. Bayly (1986) and Pierrehumbert (1986) were the first to realize that the ellipticity of those regions is responsible for three-dimensional instability and explained its mechanism. This, now known as the elliptical instability, is a linear instability of the Euler flow with elliptical streamlines and constant vorticity with respect to perturbations in the form of inertial waves (common in geo- and astrophysics). This problem was intensively investigated in the last decades,

† Email address for correspondence: krzystof.mizerski@gmail.com

and different factors like viscosity (Landman & Saffman 1987) and nonlinear effects (Lebovitz & Saldanha 1999) were taken into account, also in magnetohydrodynamic context (Thess & Zikanov 2007). In the aeronautic context, a mechanism based on elliptical instability was used to explain the three-dimensional turbulence generation for co-rotating and counter-rotating vortex pairs (Leweke & Williamson 1998; Meunier & Leweke 2001; Le Dizes & Laporte 2002; Sipp & Jacquin 2003; Fabre & Jacquin 2004; Meunier, Le Dizès & Leweke 2005). Craik (1986, 1988, 1989) and Craik & Criminale (1986) analysed turbulence development via three wave resonances and the evolution of perturbations in a shear flow in the presence of Coriolis force and also for electrically conducting fluid interacting with external magnetic field. However, our main motivation for the study of the influence of the Lorentz and Coriolis forces on the stability of elliptical vortices comes from geo- and astrophysics. Approximately elliptical shape caused by tidal forces is very common in many real astrophysical systems such as planetary cores, binary stars and accretion discs. The development of hydrodynamic instabilities in such systems has direct implications for the problem of generation of the planetary and stellar magnetic fields and for the analysis of propagation of magnetohydrodynamic waves which on the surface are seen as specific oscillations of the magnetic field. In the case of liquid planetary cores the stability problem of the flow inside them has important consequences for the processes of torque exchange with the neighbouring elliptically deformed solid body – the mantle in the geophysical context. Understanding and providing a coherent description of those processes is a base for creating a detailed model of the precessional motion of the Earth and the length of day variations. This is why the elliptical instability has also significant implications in geophysics, planetology and astrophysics.

Suess (1970) showed that the tidal forces of Moon and Sun tend to establish an elliptical flow in the Earth's core. At the same time gravimetric measurements (Melchior & Ducarme 1986; Aldridge & Lumb 1987; Melchior *et al.* 1988; Crossley, Hinderer & Legros 1991) suggest the presence of inertial waves in the liquid core. On this basis Kerswell (1994) analysed the possibility of elliptical instability development, leading to the growth of those waves in the Earth's core, in the presence of the Coriolis force and toroidal magnetic field. He found that even small elliptical deformation is sufficient for resonant excitation of inertial modes, which are not damped by diffusive effects. The presence of such magnetic waves at the core–mantle boundary (CMB) may also be detected through the analysis of the magnetic field oscillations at the surface, as well as the oscillations in the spinning and precessing motion of the Earth, which they trigger (Braginsky 1999).

One of the very important issues in geophysics is the problem of the Earth's magnetic field generation, i.e. the dynamo effect in the liquid outer core (Braginsky 1991; Soward 1991; Roberts & Soward 1992). The process which is most often proposed to be responsible for the generation of planetary magnetic fields is convection (thermal and/or compositional) in an electrically conducting fluid of the planetary cores. However, recently Le Gal, Lacaze & Le Dizès (2005) and Lacaze *et al.* (2006) have shown the feasibility of an alternative mechanism, based on the above-mentioned resonant amplification of inertial waves, caused by tidal (elliptical) deformation of planetary cores. These results are of particular interest in the context of the recent Galileo mission, which revealed that Jupiter's two satellites – Io and Ganymede – have their own magnetic fields. In both cases the magnetic field generation cannot be explained by convective mechanism. In Io convection is very unlikely because of strong tidal heating of its mantle, caused by the proximity of Jupiter (Wienbruch & Spohn 1995), while the small size of Ganymede makes sustenance of convection for

billions of years very implausible. Kerswell & Malkus (1998), taking into account the significance of the tidal forces in those satellites, suggested that their magnetic fields are an outcome of tidal (elliptical) instabilities and claimed that they are very likely to occur in those bodies. For the Earth the mechanism of magnetic field generation via the inertial instabilities resulting from precession of the Earth's rotation axis or from the tidal forces was proposed earlier (Vanyo *et al.* 1995; Kerswell & Malkus 1998; Noir *et al.* 2001; Tilgner 2005), also as a possible mechanism of induction of the magnetic field at an early stage, before the start of crystallization of the inner core about one billion years ago.

In relation to the dynamics of ocean and atmosphere Miyazaki & Fukumoto (1992) and Miyazaki (1993) investigated the influence of the Coriolis force and density stratification, caused by temperature or salinity gradient, on the elliptical instability. The results of the analysis of this instability type are also of potential interest in the context of the solar wind transport through the magnetopause. This is a region in which the solar wind, carrying the solar magnetic field, encounters the magnetic field of the Earth generating strong shear and triggering the Kelvin–Helmholtz instability, which, as it develops, creates elliptically shaped vortex structures (Le Dizes 2003), on which fully three-dimensional instabilities develop (Pierrehumbert 1986). Roth *et al.* (2001), Mozer, Phan & Bale (2003) and Hasegawa (2005) have shown that the destabilization of the magnetopause is necessary to explain the effective transport of the solar wind to the magnetosphere (and then to the ionosphere as manifested by the associated aurora phenomenon).

A very important issue in astrophysics is that of the angular momentum transfer in accretion discs. It is believed that turbulence must be employed for a coherent description of this phenomenon. The elliptical instability, in a purely hydrodynamic context, was discussed in terms of a possible mechanism of generation of turbulence in tidally distorted accretion discs by Goodman (1993). A recent experimetal study by Ji *et al.* (2006) suggests, however, that magnetohydrodynamic turbulence must be employed in order for the angular momentum to be transported effectively. One of the mechanisms of generation of the magnetohydrodynamic turbulence, widely believed to operate in accretion discs, is the magnetorotational instability (MRI). This instability is due to the presence of the magnetic field perpendicular to the plane of an axisymmetric vortex in which angular momentum increases with distance from the centre (Balbus & Hawley 1991). Lebovitz & Zweibel (2004) proposed an alternative generative mechanism resulting from tidal deformations of the discs and the development of elliptical instability in the presence of external magnetic field. They found that when the Alfvén speed is large, $u_A \gtrsim \sqrt{3}\omega d$, where d is the vertical extent of the accretion disc and ω is its rotation rate, the elliptical instability should be damped. We show how this upper bound for the magnetic field strength above which the instability cannot operate is modified by the presence of background rotation. However, rather than looking at the problem globally, we shall have in mind the picture of an elliptically deformed vortex embedded in an accretion disc. Such vortices are created due to the shear instability of the non-uniform average angular velocity profile in the disc.

In the context of the dynamics of the solar interior Lebovitz & Lifschitz (1996) investigated the stability of the Riemann ellipsoids (the models of self-gravitating rotating stars, the problem going back to Chandrasekhar 1969), i.e. the possibility of elliptical instability taking place in the Sun's interior, in the presence of short-wavelength perturbations and in the absence of the magnetic field. Mizerski, Bajer & Moffatt (2009) studied the dynamo problem (the alpha effect) in such systems.

A review of different mechanical aspects of the elliptical instability in the theory of turbulence and in geophysics, astrophysics and planetology was done by Kerswell (2002). However, it is also worth mentioning that Le Bars & Le Dizes (2006) found the elliptical instability to be strongly affected by thermal phenomena which may lead to its suppression. They suggested that in the context of astrophysical objects (including the Earth) the thermal effects on the elliptical instability development should be taken into account.

From the point of view of geophysical and astrophysical applications it seems crucial to investigate the joint effect exerted by the Coriolis and Lorentz forces on the elliptical instability, which was not investigated so far. Lacaze *et al.* (2006) did not take into account the Coriolis force. Moreover they considered only weak magnetic fields, i.e. the *kinematic dynamo* problem, neglecting the Lorentz force. The latter was included by Lebovitz & Zweibel (2004), but they neglected the effect of the Coriolis force.

In the present paper we analyse in detail the joint influence of the background rotation (Coriolis force) and an external uniform magnetic field (Lorentz force) on the stability of the Euler flow with elliptical streamlines of a perfectly conducting fluid. We show how the growth rates of the perturbations depend on their direction of propagation and on the parameters measuring the strength of the magnetic field, the intensity of background rotation and the ellipticity of the basic flow. We also visualize the evolution of a selected unstable mode by presenting the time evolution of its magnetic field lines, streamlines and the lines of the electric current density and also the trajectories of fluid particles (Mizerski & Bajer 2007). First we describe the method we use to analyse the stability problem, and then in §3 we present the numerical solutions for various parameter values. Section 4 and the Appendix are devoted to the detailed theoretical explanation of the computed stability diagrams.

2. Formulation

We consider a linear velocity field with elliptical streamlines given by

$$\boldsymbol{u}_0 = \omega[-Ey, E^{-1}x, 0] = \gamma[-(1+\epsilon)y, (1-\epsilon)x, 0], \qquad (2.1)$$

where $\omega > 0$ is a measure of the intensity of the flow; $E \geqslant 1$ is a measure of elliptical deformation of the streamlines; $2\gamma\hat{\boldsymbol{e}}_z$ is the uniform, vertical vorticity; $-\gamma\epsilon$ is the strain rate; and $0 < \epsilon < 1$ for the flow to be elliptical. It is subject to the external uniform magnetic field $\boldsymbol{B}_0$, in a system of reference rotating with constant angular velocity $\boldsymbol{\Omega}$ (figure 1a),

$$\boldsymbol{B}_0 = B_0\hat{\boldsymbol{e}}_z, \quad \Omega = \Omega\hat{\boldsymbol{e}}_z. \qquad (2.2)$$

In this paper we study the linear stability of the above system, by analysing the evolution of the three-dimensional perturbations of the velocity field $\boldsymbol{u}'(\boldsymbol{x}, t)$ and the magnetic field $\boldsymbol{B}'(\boldsymbol{x}, t)$.

Equation (2.1) gives two equivalent forms of the velocity field. We will use both, choosing the more appropriate one depending on the context. The parameters ω and γ will be used to distinguish between the two conventions; i.e. the first one will be called the *intensity convention* and the other the *vorticity convention*. (In general the vorticity convention is more natural and suitable for the stability analysis of the system. In the intensity convention the limit of the plane shear flow – which, since Kelvin 1887, is known to be linearly stable but algebraically unstable – naturally takes the form $E \to \infty$ where Ω is constant. Such limit is singular because the vorticity and the strain rate tend to infinity. In the vorticity convention, however, this limit is

Intensity convention	Vorticity convention
Intensity of the flow	Vorticity of the flow
$\omega = \gamma\sqrt{1-\epsilon^2}$	$\gamma = \dfrac{1}{2}\omega(E+E^{-1}) = \omega\delta$
Measure of ellipticity	Strain
$E = \sqrt{\dfrac{1+\epsilon}{1-\epsilon}} = \delta + \sqrt{\delta^2-1}$	$\epsilon = \dfrac{E^2-1}{E^2+1} = \dfrac{\zeta}{\delta}$
The ratio of the background rotation to the intensity	Inverse of the Rossby number
$\mathscr{R}_i \doteq \dfrac{\Omega}{\omega} = \mathscr{R}_v\delta$	$\mathscr{R}_v \doteq Ro^{-1} = \dfrac{\Omega}{\gamma}$
Dimensionless magnitude of the magnetic field	Dimensionless magnitude of the magnetic field
$H = \dfrac{k_0 B_0}{\sqrt{\mu_0\rho\omega}} = h\delta$	$h = \dfrac{k_0 B_0}{\sqrt{\mu_0\rho\gamma}}$

TABLE 1. Table of parameters where μ_0, $\rho = $ const. and k_0^{-1} are magnetic permeability of vacuum, constant density of the fluid and length scale of the perturbations, respectively.
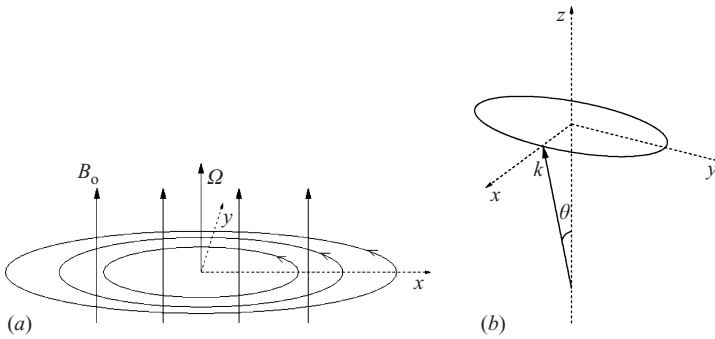

FIGURE 1. A schematic drawing of (*a*) the basic state – planar flow with elliptical streamlines in the presence of a vertical uniform magnetic field in a system of reference rotating with angular velocity Ω – and (*b*) the time evolution of the wave vector $\boldsymbol{k}$ of the perturbations – the end of the wave vector moves along an ellipse rotated by an angle $\pi/2$ with respect to the streamlines of the basic flow $\boldsymbol{u}_0$.

naturally given by $\epsilon \to 0$ where γ is constant. On the other hand the parameter ω is the basic frequency of the motion of a fluid particle along elliptical trajectories, and therefore the intensity convention seems more suitable for analysing resonant destabilization in §4.) Below we list the full set of the parameters which are going to be used throughout this paper and the relations between them:

$$\zeta \doteq \frac{1}{2}(E-E^{-1}) = \frac{\epsilon}{\sqrt{1-\epsilon^2}}, \quad \delta \doteq \frac{1}{2}(E+E^{-1}) = \frac{1}{\sqrt{1-\epsilon^2}}, \tag{2.3}$$

See table 1.

The equations describing the evolution of the velocity field $\boldsymbol{u}(\boldsymbol{x}, t)$ and the magnetic field $\boldsymbol{B}(\boldsymbol{x}, t)$, for an ideal, perfectly conducting fluid are the Euler's equation with the Lorentz and Coriolis forces and the induction equation,

$$\frac{\partial \boldsymbol{u}}{\partial t} + (\boldsymbol{u}\cdot\nabla)\boldsymbol{u} = -\frac{1}{\rho}\nabla p - 2\Omega\times\boldsymbol{u} + \frac{1}{\rho}\boldsymbol{j}\times\boldsymbol{B}, \tag{2.4}$$

$$\frac{\partial \boldsymbol{B}}{\partial t} + (\boldsymbol{u} \cdot \nabla) \boldsymbol{B} = (\boldsymbol{B} \cdot \nabla) \boldsymbol{u}, \tag{2.5}$$

where p is the pressure modified by the centrifugal potential $(1/2)\rho \, (\boldsymbol{\Omega} \times \boldsymbol{x})^2$, while $\boldsymbol{j}$ is density of the electric current, together with the mass conservation law

$$\nabla \cdot \boldsymbol{u} = 0 \tag{2.6}$$

and the Maxwell laws

$$\nabla \cdot \boldsymbol{B} = 0, \tag{2.7}$$

$$\boldsymbol{j}(\boldsymbol{x}, t) = \frac{1}{\mu_0} \nabla \times \boldsymbol{B}(\boldsymbol{x}, t), \tag{2.8}$$

with the displacement currents neglected. Introducing in the system small, three-dimensional perturbations $\boldsymbol{u}(\boldsymbol{x}, t) = \boldsymbol{u}_0(x, y) + \boldsymbol{u}'(\boldsymbol{x}, t)$, $\boldsymbol{B}(\boldsymbol{x}, t) = \boldsymbol{B}_0 + \boldsymbol{B}'(\boldsymbol{x}, t)$ and $p(\boldsymbol{x}, t) = p_0(x, y) + p'(\boldsymbol{x}, t)$, in the form of inertial waves, for which the direction and the speed of propagation depend on time

$$\begin{pmatrix} \boldsymbol{u}' \\ \boldsymbol{B}' \\ p' \end{pmatrix} = \begin{pmatrix} \boldsymbol{v}(t) \\ \boldsymbol{b}(t) \\ \widetilde{p}(t) \end{pmatrix} \exp[\mathrm{i}\boldsymbol{k}(t \cdot \boldsymbol{x}], \tag{2.9}$$

where $\boldsymbol{v}(\cdot)$, $\boldsymbol{b}(\cdot)$, $\widetilde{p}(\cdot)$ and $\boldsymbol{k}(\cdot)$ are functions of time only, with the pressure in the unperturbed state

$$\begin{aligned} p_0(x, y) &= \frac{1}{2}\rho\omega^2(x^2 + y^2) + \rho\Omega\omega(E^{-1}x^2 + Ey^2) \\ &= \left(\frac{1}{2}\rho\omega^2 + \rho\Omega\gamma\right)(x^2 + y^2) - \epsilon\rho\Omega\gamma(x^2 - y^2), \end{aligned} \tag{2.10}$$

the above equations take the following form:

$$\frac{\mathrm{d}\boldsymbol{v}}{\mathrm{d}t} + \mathrm{i}\boldsymbol{v}\left[\left(\frac{\mathrm{d}\boldsymbol{k}}{\mathrm{d}t} + \widehat{A}^T\boldsymbol{k}\right) \cdot \boldsymbol{x}\right] = -\widehat{A}\boldsymbol{v} - \mathrm{i}\boldsymbol{k}\frac{\widetilde{p}}{\rho} - 2\widehat{O}\boldsymbol{v} + \frac{\mathrm{i}B_0}{\mu_0\rho}(\boldsymbol{k} \times \boldsymbol{b}) \times \hat{\boldsymbol{e}}_z, \tag{2.11}$$

$$\frac{\mathrm{d}\boldsymbol{b}}{\mathrm{d}t} + \mathrm{i}\boldsymbol{b}\left[\left(\frac{\mathrm{d}\boldsymbol{k}}{\mathrm{d}t} + \widehat{A}^T\boldsymbol{k}\right) \cdot \boldsymbol{x}\right] = \widehat{A}\boldsymbol{b} + \mathrm{i}k_z B_0\boldsymbol{v}, \tag{2.12}$$

$$\boldsymbol{k} \cdot \boldsymbol{v} = 0, \quad \boldsymbol{k} \cdot \boldsymbol{b} = 0, \tag{2.13}$$

where $\widehat{A}$ is the gradient of the basic velocity field $\boldsymbol{u}_0$,

$$\boldsymbol{u}_0 = \widehat{A}\boldsymbol{x}; \quad \text{so} \quad \widehat{A} = \omega\begin{bmatrix} 0 & -E & 0 \\ E^{-1} & 0 & 0 \\ 0 & 0 & 0 \end{bmatrix} = \gamma\begin{bmatrix} 0 & -(1+\epsilon) & 0 \\ (1-\epsilon) & 0 & 0 \\ 0 & 0 & 0 \end{bmatrix}, \tag{2.14}$$

and operator $\widehat{O} = \boldsymbol{\Omega} \times$,

$$\widehat{O} = \Omega\begin{bmatrix} 0 & -1 & 0 \\ 1 & 0 & 0 \\ 0 & 0 & 0 \end{bmatrix}. \tag{2.15}$$

Since the terms proportional to $\boldsymbol{x}$ in (2.11) and (2.12) must balance separately, we obtain the equation

$$\frac{\mathrm{d}\boldsymbol{k}}{\mathrm{d}t} = -\widehat{A}^T\boldsymbol{k}, \tag{2.16}$$

the solution of which,

$$\boldsymbol{k} = k_0 \left(\sin \vartheta \cos \left[\omega \left(t - t_0 \right) \right], E \sin \vartheta \sin \left[\omega \left(t - t_0 \right) \right], \cos \vartheta \right), \tag{2.17}$$

describes the evolution of the wave vector $\boldsymbol{k}$ along an ellipse similar to that of the basic flow streamlines but with the main axes interchanged. Here constant k_0^{-1} is the length scale of the perturbation, already used in table 1 (k_0 is the minimal norm of $\boldsymbol{k}$); angle ϑ is constant and is the minimal angle between the wave vector $\boldsymbol{k}$ and the z axis; and t_0 is an arbitrary parameter serving only to determine the phase of the wave vector $\boldsymbol{k}$ (see figure 1b).

By the use of the incompressibility condition (2.13) we may eliminate pressure from (2.11),

$$-i\frac{\widetilde{p}}{\rho} = \frac{2}{k^2} [(\widehat{A}^T + \widehat{O}^T)\boldsymbol{k}] \cdot \boldsymbol{v} + i \frac{B_0 b_z}{\mu_0 \rho}, \tag{2.18}$$

and substituting it again in the (2.11) we get

$$\frac{\mathrm{d}\boldsymbol{v}}{\mathrm{d}t} = \left[\frac{2}{k^2} \boldsymbol{k} \otimes \boldsymbol{k} (\widehat{A} + \widehat{O}) - \widehat{A} - 2\widehat{O} \right] \boldsymbol{v} + \frac{iB_0 k_z}{\mu_0 \rho} \boldsymbol{b}, \tag{2.19}$$

where $\otimes$ denotes tensor multiplication. Quite remarkably it turns out that the z components of the fields $\boldsymbol{v}$ and $\boldsymbol{b}$ are slaved (Lebovitz & Zweibel 2004), since they only appear in the z components of (2.12) and (2.19),

$$\frac{\mathrm{d}v_z}{\mathrm{d}t} = -\frac{2\omega k_z}{k^2} [(E + R_i)k_x v_y - (E^{-1} + R_i)k_y v_x] + \frac{iB_0 k_z}{\mu_0 \rho} b_z, \tag{2.20}$$

$$\frac{\mathrm{d}b_z}{\mathrm{d}t} = iB_0 k_z v_z. \tag{2.21}$$

This means that (2.20) and (2.21) can be solved for v_z and b_z after v_x, v_y, b_x and b_y are found. Another method for calculating v_z and b_z is provided by the solenoidal conditions (2.13) if $k_z \neq 0$. Moreover, from the form of these equations we easily infer that the components v_z and b_z do not influence stability, since the homogeneous system of equations (2.20) and (2.21) have only oscillatory and not exponentially growing solutions. We are, therefore, allowed to reduce the system of six equations for all the six components of $\boldsymbol{v}$ and $\boldsymbol{b}$ to a system of four equations for the components v_x, v_y, b_x and b_y.

In derivation of (2.19) we used the solenoidal conditions (2.13). This, in general, does not mean, however, that these conditions are now automatically built into the system of equations (2.19), (2.12) and (2.16). Still, these equations imply

$$\frac{\mathrm{d}}{\mathrm{d}t} (\boldsymbol{k} \cdot \boldsymbol{v}) = \frac{iB_0 k_z}{\mu_0 \rho} \boldsymbol{k} \cdot \boldsymbol{b}, \tag{2.22}$$

$$\frac{\mathrm{d}}{\mathrm{d}t} (\boldsymbol{k} \cdot \boldsymbol{b}) = iB_0 k_z \boldsymbol{k} \cdot \boldsymbol{v}, \tag{2.23}$$

and therefore it is enough to ensure that $\boldsymbol{k} \cdot \boldsymbol{v}$ and $\boldsymbol{k} \cdot \boldsymbol{b}$ vanish only at the initial instant. Then these conditions will hold for all $t > 0$ as a consequence of (2.19) and (2.12). Moreover, since the solutions of (2.22) and (2.23) are necessarily periodic in time, for the unstable, exponentially growing solutions the solenoidal conditions (2.13) are satisfied automatically.

We rewrite the system of equations (2.12) and (2.19) in the following compact form (making a simple rescaling $\boldsymbol{b} \to (1/\sqrt{\mu_0 \rho})\boldsymbol{b}$):

$$\frac{\mathrm{d}s}{\mathrm{d}\tau} = \boldsymbol{S}(\tau)\,s, \tag{2.24}$$

where

$$\tau = \omega(t - t_0), \qquad s = \begin{bmatrix} v_x \\ v_y \\ b_x \\ b_y \end{bmatrix}, \tag{2.25}$$

$$\boldsymbol{S}(\tau) = \begin{bmatrix} \dfrac{2k_x k_y}{k^2}(E^{-1} + \mathscr{R}_i) & \left(1 - \dfrac{2k_x^2}{k^2}\right)(E + \mathscr{R}_i) + \mathscr{R}_i & \mathrm{i}H\cos\vartheta & 0 \\[2mm] \left(\dfrac{2k_y^2}{k^2} - 1\right)(E^{-1} + \mathscr{R}_i) - \mathscr{R}_i & -\dfrac{2k_x k_y}{k^2}(E + \mathscr{R}_i) & 0 & \mathrm{i}H\cos\vartheta \\[2mm] \mathrm{i}H\cos\vartheta & 0 & 0 & -E \\[2mm] 0 & \mathrm{i}H\cos\vartheta & E^{-1} & 0 \end{bmatrix}. \tag{2.26}$$

It is worth pointing out that for $H = 0$ the matrix $\boldsymbol{S}$ becomes independent of k_0, which means it is only the presence of the magnetic field in the system that introduces the dependence of the stability problem on the wavelength of the perturbations.

Equation (2.24) is an ordinary first-order system of differential equations, and since the matrix $\boldsymbol{S}(\tau)$ is periodic in τ with the period of 2π, this equation constitutes a Floquet problem for vector $s(\tau)$ (Bender & Orszag 1978). The general solution of (2.24) is a linear superposition of Floquet modes

$$s(\tau) = \mathrm{e}^{\sigma\tau}\boldsymbol{f}(\tau), \tag{2.27}$$

where $\boldsymbol{f}(\tau)$ is 2π-periodic and σ is the complex growth rate, which is measured in the units of the basic flow intensity ω. The linear stability of the basic state $\boldsymbol{u}_0$, $\boldsymbol{B}_0$ depends on the existence of exponentially growing solutions of (2.24), i.e. on the sign of the real part of the Floquet exponent σ. This exponent is determined by the fundamental matrix solution $\boldsymbol{M}(\tau)$ of the differential equation (2.24), satisfying $s(\tau) = \boldsymbol{M}(\tau)\,s(\tau = 0)$, through the fact that $\exp(2\pi\sigma)$ is an eigenvalue of the matrix $\boldsymbol{M}(2\pi)$. The equation for $\boldsymbol{M}(\tau)$ is analogous to (2.24),

$$\frac{\mathrm{d}}{\mathrm{d}\tau}M_{ij} = \mathscr{S}_{ik}(\tau)M_{kj}, \tag{2.28}$$

with initial condition

$$M_{ij}(\tau = 0) = \delta_{ij}, \tag{2.29}$$

where δ_{ij} is the unit matrix. If by $\Lambda(E, \vartheta, \mathscr{R}_i, H)$ we denote the eigenvalues of $\boldsymbol{M}(2\pi)$, the growth rates are then given by

$$\sigma(E, \vartheta, \mathscr{R}_i, H) = \frac{1}{2\pi}\ln\Lambda(E, \vartheta, \mathscr{R}_i, H). \tag{2.30}$$

This means that if any of the eigenvalues satisfies $|\Lambda| > 1$ the system is unstable.

Equation (2.28) can be solved numerically to compute the matrix $\boldsymbol{M}$ at $\tau = 2\pi$ and its eigenvalues $\Lambda(E, \vartheta, \mathscr{R}_i, H)$. In the following section we present the results of such numerical analysis of the stability problem for different values of the parameters H

(magnetic field strength), $\mathscr{R}_i$ (the strength of the background rotation) and δ (the ellipticity). At the end of this section we also present the numerically calculated evolution of a typical unstable mode.

3. Numerical results

For a wide range of values of the parameters, (2.28) was solved numerically, by the Runge–Kutta method (standard MATLAB procedure *ode45*) with the initial condition given in (2.29). For each set of parameters $(\cos\vartheta, \delta, h, \mathscr{R}_v)$ the matrix $\boldsymbol{M}(2\pi)$ and its eigenvalues were computed and then, with the aid of (2.30), the maximum of the real part of the growth rate. Thanks to the symmetry $\cos\vartheta \leftrightarrow -\cos\vartheta$ of the equations of magnetohydrodynamics ((2.4) and (2.5)), it was enough to consider ϑ only in the interval $0 < \vartheta < \pi/2$. (It can be seen from (2.24) and (2.26) that the interchange $\cos\vartheta \rightarrow -\cos\vartheta$ is equivalent to $H \rightarrow -H$, i.e. the reversal of the direction of $\boldsymbol{B}_0$. The equations of magnetohydrodynamics imply that such transformation only causes the magnetic field perturbation $\boldsymbol{B}'$ to change sign but does not influence the stability problem otherwise. Therefore, we will keep the assumption $\cos\vartheta > 0$ throughout the paper; see also the discussion below (4.3) in §4. Because of its greater practical utility, the vorticity convention was used for numerical simulations, and therefore the vorticity γ is the unit of the growth rates.

We start with presenting stability diagrams in the δ–ϑ plane (figures 2 and 3) for different values of the parameters h and $\mathscr{R}_v$. The intensity of the grey colour indicates the values of the growth rates. The stable regions are marked with white, and the unstable ones typically take the form of grey wedges widening with increasing δ. First, in figure 2, we reproduce the known results for the stability of elliptical flow in a non-rotating system and with $\boldsymbol{B}_0 = 0$ (Bayly 1986) and also the effects of the background rotation (Miyazaki 1992) and the magnetic field (Lebovitz & Zweibel 2004) separately. When the magnetic field is present, not only does the single unstable wedge for $h = \mathscr{R}_v = 0$, with the apex at $(\delta = 1, \vartheta = \pi/3)$, change its location, but also new thinner unstable wedges appear, since there are more destabilizing resonances possible, between the frequencies of oscillations of the modes. This means that the presence of magnetic field allows for destabilization of the system along new directions of propagation of the perturbations. A similar effect is exerted by the background rotation, although there are fewer unstable wedges, and they are much weaker. (For $\mathscr{R}_v = 0.6$ a very thin wedge, which touches the ϑ axis at $\vartheta = \arccos(1/(2 + 2\mathscr{R}_v))$, is clearly seen.) The crucial difference, however, is that for anticyclonic rotation, i.e. for $\mathscr{R}_v < 0$, in the range $-1 < \mathscr{R}_v < 0$ a strong unstable region which is not of resonant nature appears, in which the most unstable modes are those propagating along the z axis ($\vartheta = 0$). This type of instability is explained in detail by Bajer & Mizerski (2008) in a general magnetic case. After Miyazaki (1992) it is called the *horizontal instability*, since for $\vartheta = 0$ the perturbations of the velocity and the magnetic field lie in the horizontal xy plane. For $h = 0$ and $-1 < \mathscr{R}_v < 0$, the instability appears only for ellipticities δ greater then a critical value, $\delta_c = 1/\sqrt{-4\mathscr{R}_v(\mathscr{R}_v + 1)}$. Additionally, in the presence of Coriolis force, the unstable regions may take the form of wedges with apexes on the δ axis and widening with increasing ϑ and δ (see figure 2e). Only this type of unstable regions is possible for $-3/2 < \mathscr{R}_v < -1/2$. The stability characteristics of strong anticyclonic vortices (weak anticyclonic rotation), $\mathscr{R}_v < -3/2$, become similar to those of cyclonic vortices ($\mathscr{R}_v > 0$).

The joint influence of the Coriolis and Lorentz forces can be seen in figure 3. Weak background rotation, in the presence of external magnetic field, does not bring
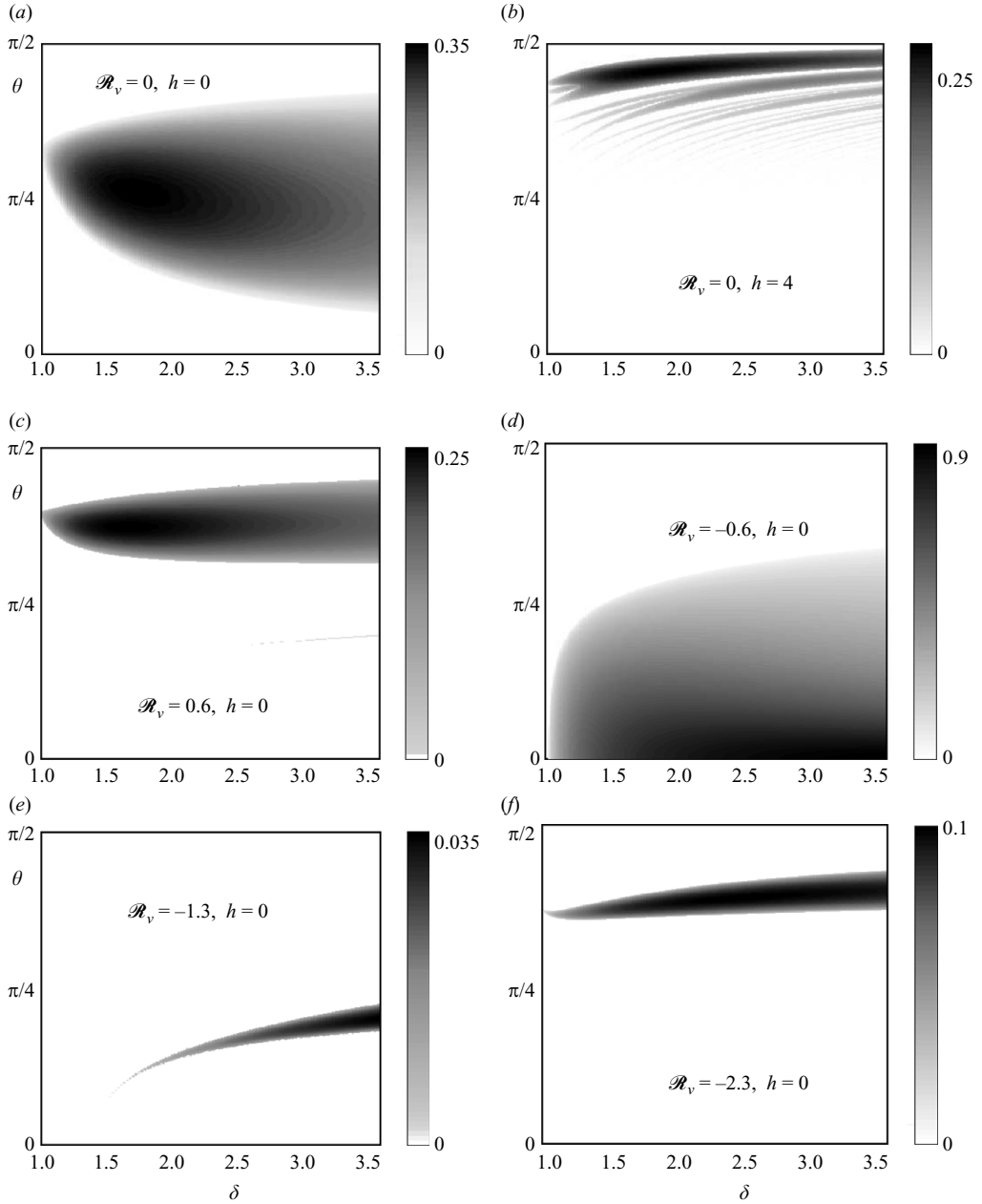
FIGURE 2. Greyscale maps of growth rates in the $\delta-\vartheta$ plane: (a) $h=0$, $\mathscr{R}_v=0$; (b) $h=4$, $\mathscr{R}_v=0$; (c) $h=0$, $\mathscr{R}_v=0.6$; (d) $h=0$, $\mathscr{R}_v=-0.6$; (e) $h=0$, $\mathscr{R}_v=-1.3$; (f) $h=0$, $\mathscr{R}_v=-2.3$. The main effect of the Lorentz force is the breakup of one unstable wedge into many smaller wedges (larger number of destabilizing resonances at $\delta=1$) and its shift towards higher values of the angle ϑ. The Coriolis force in the range $-1<\mathscr{R}_v<0$ causes the horizontal instability (Bajer & Mizerski 2009), which typically has very large growth rates and for $\mathscr{R}_v<-1$ allows for resonant destabilization of some ellipticities δ.
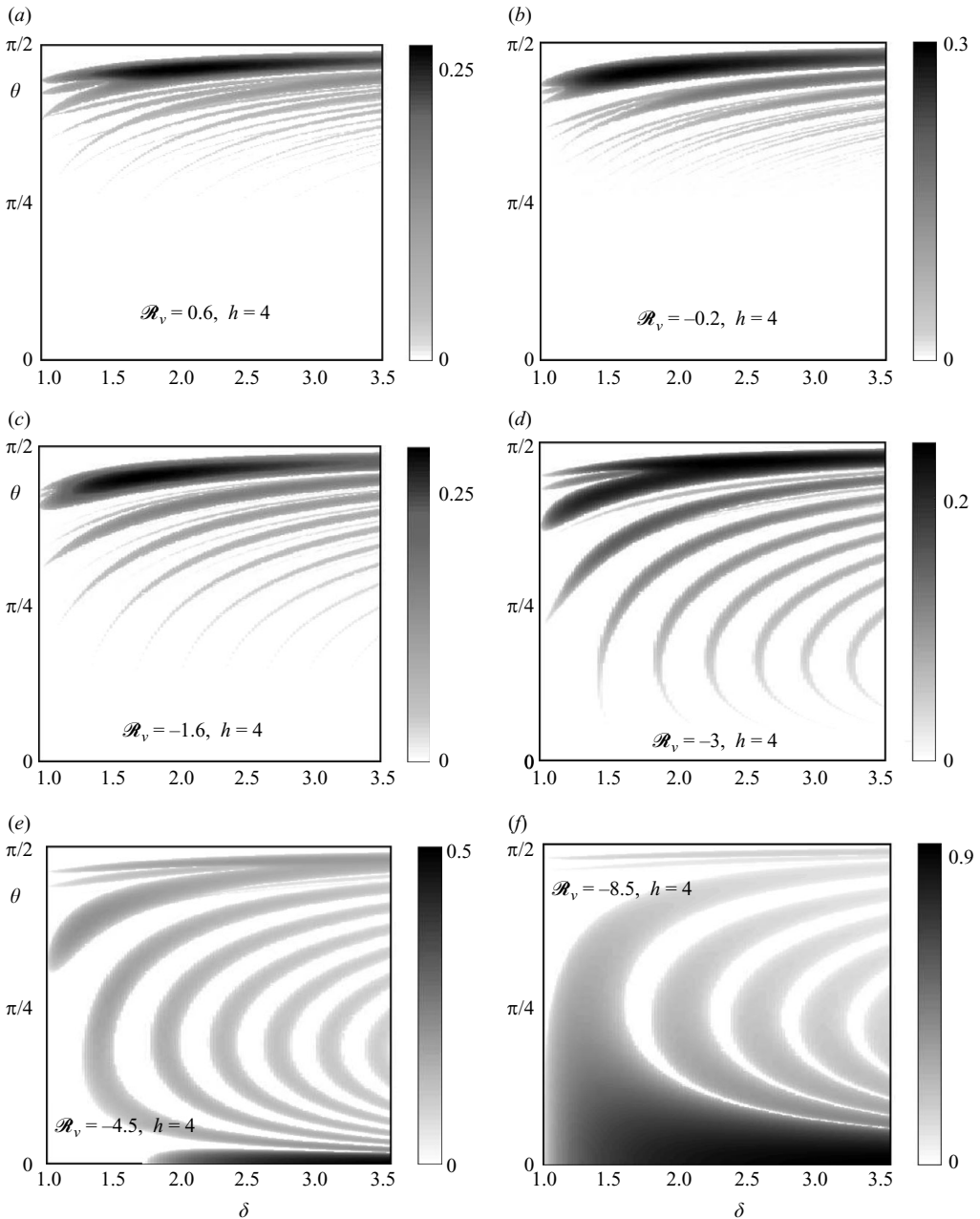
FIGURE 3. Grey-shaded maps of growth rates in $\delta-\vartheta$ plane – the joint effect of the Coriolis and Lorentz forces: $(a)\,h=4,\,\mathscr{R}_v=0.6;$ (b) $h=4,\,\mathscr{R}_v=-0.2;$ $(c)\,h=4,\,\mathscr{R}_v=-1.6;$ (d) $h=4,\,\mathscr{R}_v=-3.0;$ (e) $h=4,\,\mathscr{R}_v=-4.5;$ and (f) $h=4,\,\mathscr{R}_v=-8.5.$ The Lorentz and the Coriolis forces together create more resonantly destabilized modes (i.e. destabilized by resonances between their frequencies of oscillation) and widen the range of existence of horizontal instability to an unbounded interval $\mathscr{R}_v < -h^2/4.$

in any significantly new stability characteristics, but clearly, weak cyclonic rotation tends rather to change the shapes of the unstable regions, whereas weak anticyclonic rotation tends to decrease the growth rates (compare figures 2b, 3a and 3b). Both factors, jointly and separately, cause the directions of propagation of the resonant unstable modes to tend to the vertical (z) axis; in other words the wedges with apexes on the ϑ axis move upwards with increasing h or $\mathcal{R}_v$. For all values of $\mathcal{R}_v$ the apexes of the thickest unstable wedges at $\delta = 1$ are given in (4.5), (4.9) and (4.16), in §4. For $0 > \mathcal{R}_v > -h^2/4$ (figures 3c and 3d), we clearly see wedges originating from the δ axis, indicating that some values of ellipticity δ are subject to destabilization via, possibly, a resonant mechanism. When $\mathcal{R}_v$ tends to $-h^2/4$ from above, the apexes of these wedges move towards infinity and reach it when $\mathcal{R}_v \leqslant -h^2/4$, making the wedges bend in a 'bow-shaped' manner. In the case in which $h = 0$ and $-1 < \mathcal{R}_v < 0$, i.e. when the horizontal instability is present in non-magnetic case, such bow shapes do not appear at all. For the wedges that originate from the δ axis, formulae analogous to (4.5), (4.9) and (4.16) could, in principle, be derived. Analysis similar to that for $\zeta \ll 1$ presented in the Appendix could be done for $\vartheta \ll 1$. However, it would be necessary to go to the order higher than ϑ^2; hence the analysis would be much more complicated. Moreover, the usefulness of the results of such analysis would probably be limited, since there are not many systems in which the direction of propagation of the perturbations is restricted to the z axis and its neighbourhood. Additionally, the growth rates inside these wedges typically are very small close to the apex. We therefore do not perform such analysis and only anticipate that the destabilization in the case of wedges originating at $\vartheta = 0$ is also due to a resonant mechanism, i.e. the resonances between the frequencies of oscillation of the horizontal modes $\varpi = \pm \gamma \sqrt{\chi_{\pm}^2 - \epsilon^2}$, where $\chi_{\pm} = \mathcal{R}_v \pm \sqrt{(\mathcal{R}_v + 1)^2 + h^2}$ (Bajer & Mizerski 2009), and the basic frequency ω. Such resonances lead to the following expressions:

$$\left.\begin{aligned} \pm\gamma\sqrt{\chi_{+}^2 - \epsilon^2} = n\omega, \quad n \in \mathbb{N} \Rightarrow \delta = \sqrt{\frac{n^2 - 1}{\chi_{+}^2 - 1}} \ \text{and} \ n \geqslant |\chi_{+}| \ \text{for} \ |\chi_{+}| > 1 \\ \text{and} \ \pm\gamma\sqrt{\chi_{-}^2 - \epsilon^2} = n\omega, \quad n \in \mathbb{N} \Rightarrow \delta = \sqrt{\frac{n^2 - 1}{\chi_{-}^2 - 1}} \ \text{and} \ n \geqslant |\chi_{-}|. \end{aligned}\right\} \quad (3.1)$$

However, it must be noted that without a proper asymptotic analysis for ($\vartheta \ll 1$) we cannot distinguish which of these resonances leads to instability, and most likely not all of them do. Moreover the resonant destabilization of the system may also be due to the resonances of the type $\varpi_j - \varpi_k = n\omega$, where $n \in \mathbb{N}$, which in some cases reduce to the conditions (3.1). The conditions for the resonance of order n in (3.1) result from the fact that $\delta \geqslant 1$. It is also worth pointing out that the first formula in (3.1) allows for resonant destabilization only if $|\chi_{+}| > 1$, i.e. in absence of the horizontal instability (Bajer & Mizerski 2009). It also explains the shift of the apexes of the unstable wedges along the δ axis towards infinity, when $\mathcal{R}_v \rightarrow -h^2/4$ from above, since then $\chi_{+} \rightarrow 1$. The second formula in general allows for resonant destabilization even if $\mathcal{R}_v$ and h are such that the horizontal instability is possible, since $|\chi_{-}| > 1$ always. In practice, however, because χ_{-} increases quickly with negative and decreasing $\mathcal{R}_v$, the condition $n \geqslant |\chi_{-}|$ makes only high resonances possible, which are likely to be weak and difficult to spot. (Such wedges may exist but may simply be too thin and the growth rates inside them too small to be detected.) For $h = 0$ and negative $\mathcal{R}_v$ the resonant excitation of horizontal modes is possible only if $\mathcal{R}_v < -1$.

As already mentioned, the Coriolis force is a reason for the existence of horizontal instability (Bajer & Mizerski 2009), which appears when $\mathcal{R}_v < -h^2/4$
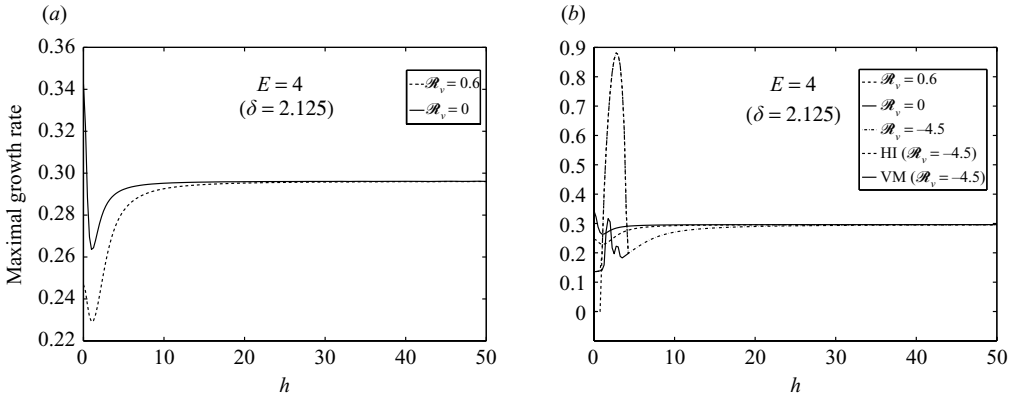
FIGURE 4. The dependence of the maximal growth rate on the dimensionless intensity of the magnetic field h for $E = 4$ and $\mathscr{R}_v = 0.6$, 0 and -4.5. In the latter case the growth rates of the vertical mode (VM) and horizontal mode (HI) are indicated separately. The limiting value $\sigma(h)$ when $h \to \infty$ is the same in all cases. A characteristic minimum at about $h \approx 2$ appears.

and is present for $\delta \geqslant 1/\sqrt{1 - \chi_+^2}$, *strongly dominating* other unstable modes. When $\mathscr{R}_v = -(h^2 + 1)/2 = -8.5$, it is present for all values of δ. We emphasize that the horizontal instability, although caused by the presence of the Coriolis force, is very strongly modified by the magnetic field. In the $h = 0$ case this type of instability may develop only in a bounded range of values of the parameter $\mathscr{R}_v$, i.e. for $-1 < \mathscr{R}_v < 0$. Switching on the magnetic field results in immediate change in the range of its existence to an unbounded interval $-\infty < \mathscr{R}_v < -h^2/4$.

Figure 4 illustrates the dependence of the growth rate maximized over the angle ϑ on the intensity h of the external magnetic field, for positive and negative values of the parameter $\mathscr{R}_v$ and also for $\mathscr{R}_v = 0$. For $\mathscr{R}_v < 0$, in the range of domination of the horizontal instability, we have also plotted the maximal growth rate for angles ϑ in the interval $\vartheta \in (\pi/4, \pi/2)$, denoted as VM (*vertical mode*). The growth rates of the horizontal perturbations are marked by HI. When $\mathscr{R}_v > -4.5$, the function $(\mathrm{Re}\,\sigma)_{max}(h)$ has a minimum at $h \approx 2$. The presence of horizontal instability significantly changes the character of this function, causing a maximum at $h \approx 3$. For all values of the parameter $\mathscr{R}_v$ presented in the limit $h \to \infty$ the growth rates tend to the same value, depending only on the ellipticity of the basic flow. (Likewise in the asymptotic case $\zeta = (1/2)(E - E^{-1}) \ll 1$, investigated in detail in the next section and the Appendix, where in the limit of strong magnetic field the growth rates tend to $(1/4)\zeta$).

In an analogous way to $(\mathrm{Re}\,\sigma)_{max}(h)$ we computed the dependencies of the growth rate, again maximized over ϑ, on the ellipticity ϵ (figure 5a) and on the parameter measuring the strength of the Coriolis force $\mathscr{R}_v$ (figure 5b). Again, in the range of existence of horizontal instability the growth rates of horizontal instability and vertical modes are plotted. It is clear that in the absence of horizontal instability the Coriolis and Lorentz forces act to decrease the growth rates, and in the limit of pure shear flow $\epsilon \to 1$, the system is then linearly stable (see figure 5a). The horizontal instability, when present, changes these characteristics completely by significant increase of the maximal growth rate and strong destabilization in the pure shear flow limit. Figure 5(b) clearly shows the domination of horizontal instability over other types of unstable modes. The values of the growth rates are definitely largest when horizontal instability is present. This means that real systems with anticyclonic rotation and
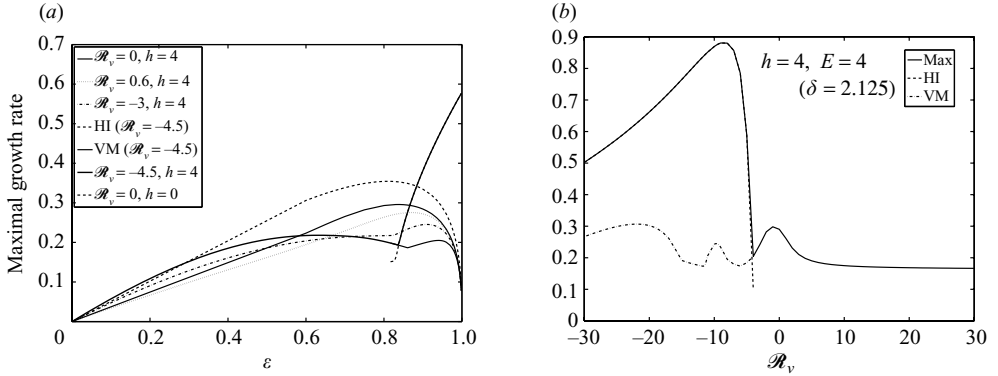
FIGURE 5. Dependence of the maximal growth rate on the ellipticity ϵ for $h = 4$ and $\mathcal{R}_v = 0$, 0.6, -3.0 and -4.5. Analogous dependence for $h = 0$ and $\mathcal{R}_v = 0$ is shown for comparison. For $\mathcal{R}_v = -4.5$ the growth rates of vertical mode (VM) and horizontal mode (HI) are shown as well in (*a*). The magnetic field and background rotation in general act to decrease growth rates, with the exception of the horizontal instability, for which the growth rates are usually very large. For large and increasing ellipticities, i.e. in the pure shear limit, in absence of HI the growth rates tend to zero. Horizontal instability, in the limit $\epsilon \to 1$, persists. (*b*) Depiction of the dependence of the maximal growth rate on the parameter $\mathcal{R}_v$ for $h = 4$ and $E = 4$. In the range of existence of the horizontal instability the growth rates of VM and horizontal mode (HI) are indicated as well. For anticyclonic rotation, when HI is present, the maximal growth rates are significantly larger than in the case of cyclonic rotation.

$\mathcal{R}_v < -h^2/4$ are more likely to develop turbulence, since the dissipative effects would have to be very strong to damp the instability.

The irregular dependence of the maximal growth rate of the vertical-mode-type perturbations on the parameters h, ϵ and $\mathcal{R}_v$ is probably a result of interaction of different modes. For $\vartheta \in (\pi/4, \pi/2)$ the unstable regions in δ–ϑ plane, originating from different types of resonances, merge with increasing δ, which influences the value of the maximal growth rate.

The above analysis sums up to the conclusion that the presence of the magnetic field and background rotation exerts a stabilizing effect by decreasing the values of growth rates in the absence of horizontal instability. This means that the viscosity and electric resistivity may damp the elliptical instability more easily if the Lorentz and/or Coriolis forces are present in the system and $\mathcal{R}_v > -h^2/4$. Additionally the whole area of the unstable regions in the δ–ϑ plane is, under these conditions, smaller than in the absence of the magnetic field and background rotation. Both statements change radically when horizontal instability enters the dynamics, since the unstable horizontal modes typically have very large growth rates, and the total area of unstable regions is also significantly larger. Moreover, besides those two effects, there is also another one, which should rather be regarded as destabilizing, since the presence of the magnetic field and background rotation allow for destabilization along new directions of propagation of the perturbations.

We end the numerical analysis with presenting the evolution of a selected unstable mode in figure 6, for $\mathcal{R}_i = 0$. For different times within one period the projections of the streamlines on the xy plane as well as the projections of the magnetic lines and lines of electric current on the xz plane are shown (figure 6*a*). It can be seen that the streamlines are being twisted as they evolve, while the electric current, $\boldsymbol{j} = \mathrm{Re}(\mathrm{i}\boldsymbol{k} \times \boldsymbol{B}')$, flows along straight lines, perpendicular to the wave vector $\boldsymbol{k}$ and
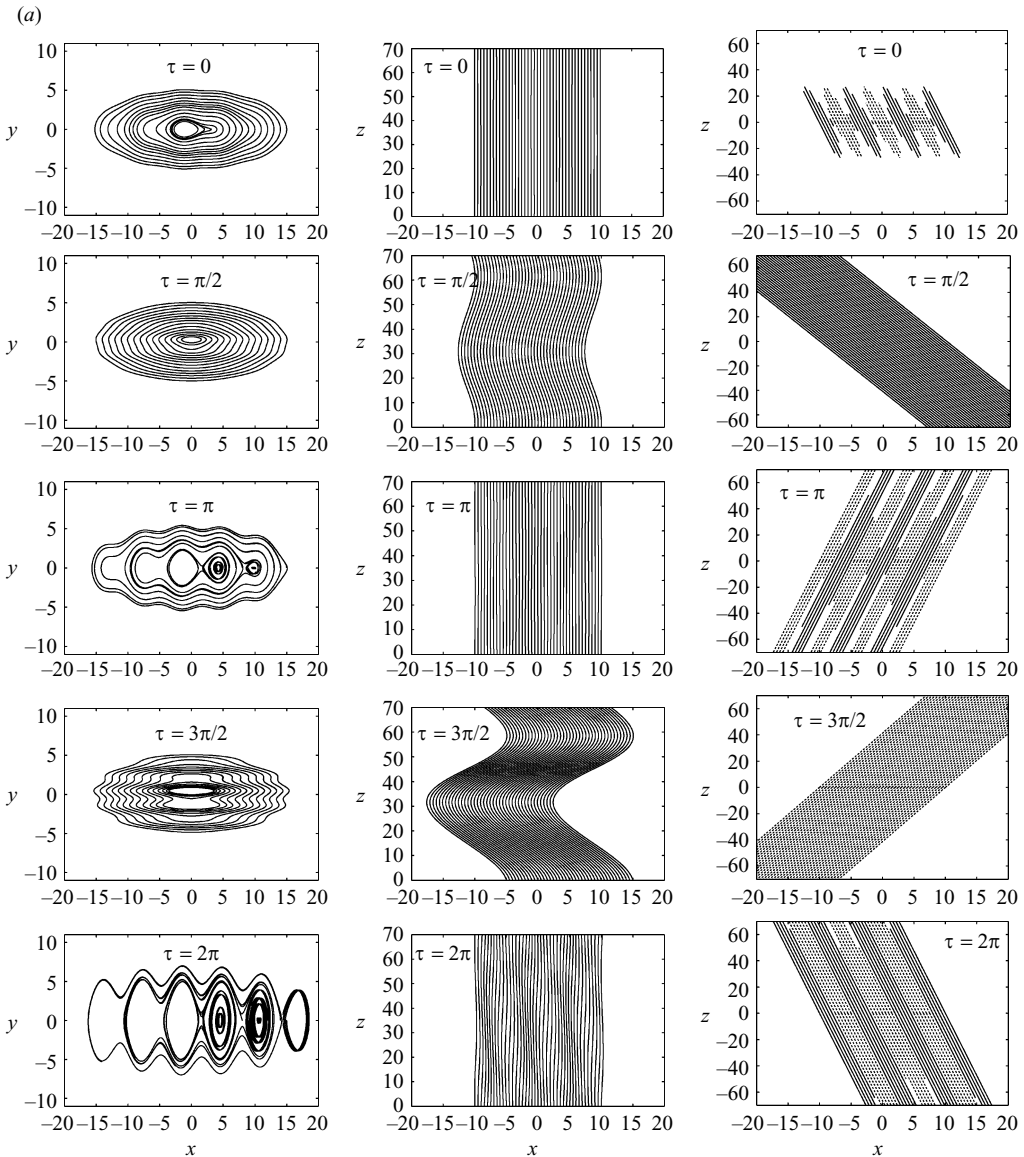
(*a*)

FIGURE 6. For legend see next page.

Im$\boldsymbol{B}'$. In figure 6(*b*) we present the three-period evolution of the projections of the trajectories of a selected fluid particle on the xy, xz and yz planes, successively after each period $T = 2\pi/\omega$. Since we visualize here the evolution of perturbations in infinite space, the initial amplitude of the perturbations is arbitrary. This is because in the case of infinite space the individual Floquet modes are exact solutions also of the fully nonlinear system of evolution equations, since the divergence-free conditions (2.13) ensure vanishing of the nonlinear terms. Thus e.g. the velocity trajectories are simply calculated in the following way: $\mathrm{d}\boldsymbol{x}/\mathrm{d}\tau = \boldsymbol{u}_0 + \mathrm{Re}\{\boldsymbol{v}(\tau)\exp[\mathrm{i}\boldsymbol{k}(\tau)\cdot\boldsymbol{x}]\}$, where the horizontal component of the initial amplitude $\boldsymbol{v}(\tau = 0)$ is obtained from the Floquet analysis, by taking the first two components of the eigenvector $\boldsymbol{s}(\tau = 0)$
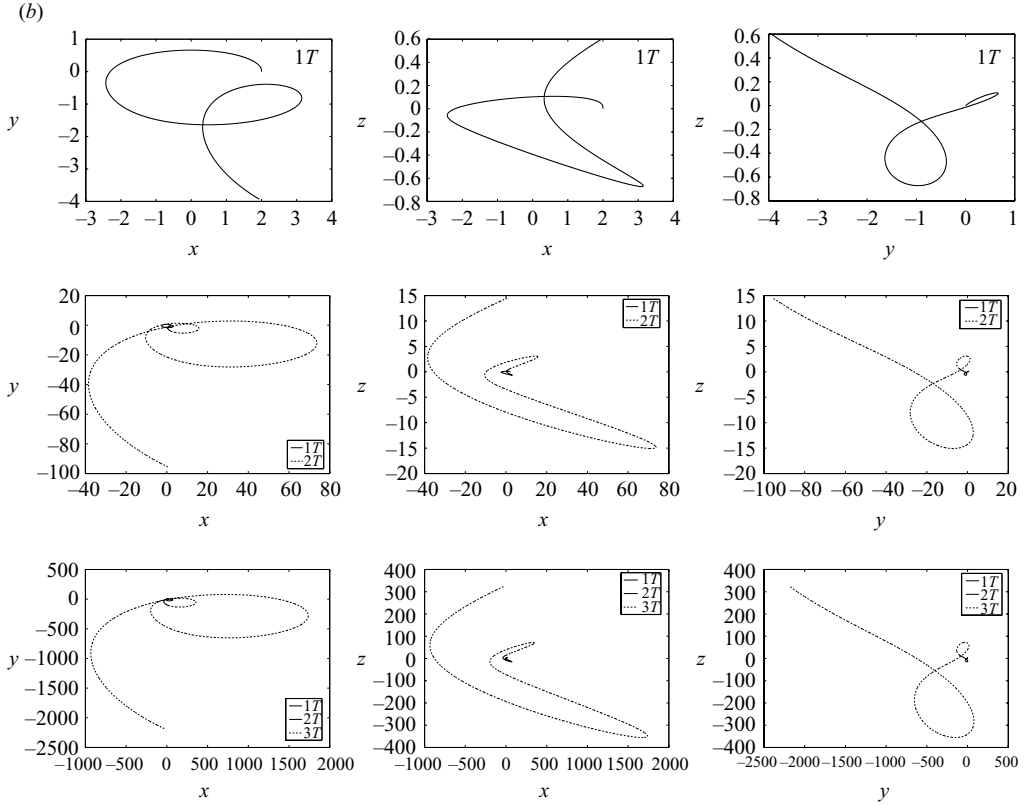
FIGURE 6. Visualization of the evolution of a selected unstable mode for $H = 4$ ($h = 1.88$) and $\mathcal{R}_v = 0$, $E = 4$: (a) projections of streamlines on the xy plane and projections of the magnetic field lines and electric current density lines on the xz plane in the perturbed flow (from left to right), at times $\tau = 0$, $\pi/2$, π, $3\pi/2$, 2π (from top to bottom). For electric current lines the direction of the current flow is indicated: continuous lines, positive; dashed lines, negative; the length of the line is correlated with the value of the vector $\boldsymbol{j}$. (b) Projections of the trajectories of a selected fluid particle on the xy, xz and yz planes (from left to right), after each of three successive periods $T = 2\pi/\omega$, i.e. for $\tau = T$, $2T$, $3T$ (from top to bottom).

of the Floquet matrix $\boldsymbol{M}(2\pi)$. We checked that the numerical solutions satisfy the solenoidal conditions for $\boldsymbol{u}$ and $\boldsymbol{B}$ (2.13).

We now proceed to the detailed explanation of the instability mechanism in the analysed system. In the next section we will answer the question which of the perturbations of a circular flow are destabilized in consequence to small deviations of the basic flow from axial symmetry.

4. The destabilizing resonances

In the Appendix we will repeat the whole procedure of the asymptotic calculation for $\zeta \ll 1$ done by Lebovitz & Zweibel (2004) for $\mathcal{R}_i = 0$ but with the inclusion of Coriolis force. Here we only state the results. First we note that the time average of the trace of $\boldsymbol{S}(\tau)$ over a period $(1/2\pi)\int_0^{2\pi}\mathrm{Tr}(\boldsymbol{S}(\tau))\mathrm{d}\tau = 0$; thus the Liouville theorem gives $\det(\boldsymbol{M}(2\pi)) = 1$. Hence our system is conservative and possesses the property that if Λ is an eigenvalue of the Floquet matrix $\boldsymbol{M}(2\pi)$, so is its inverse Λ^{-1} and its complex conjugate Λ^*. The proof of this fact is exactly the same as given by

Lebovitz & Zweibel (2004), and we will not repeat it here. This implies that in the stable situation all eigenvalues of $\boldsymbol{M}(2\pi)$ must lie on the unit circle. Moreover, at the instability threshold, when the eigenvalue Λ is about to leave the unit circle, its multiplicity is at least 2, since the eigenvalue $(\Lambda^*)^{-1}$ must leave the unit circle simultaneously, and on the unit circle, at the threshold, $\Lambda = (\Lambda^*)^{-1}$. This means that the destabilization of Floquet modes is a result of a special type of resonances between them (including resonances between their frequencies and the basic frequency ω). For $\zeta = 0$, i.e. when the streamlines of the basic flow are circular, these resonances are defined by the condition $\varpi_k - \varpi_l = n$, with $n \in \mathbb{N}$, where the frequencies ϖ_j, $j = 1, 2, 3, 4$, are defined in (4.3). If $n \neq \pm 2$ the matrix $\boldsymbol{J}'$ defined in the Appendix is diagonal (see the discussion after (A 28)). The roots of (A 40) take the following, purely imaginary, form:

$$\Gamma \in \left\{ \frac{1}{\lambda_k}(\boldsymbol{M}'_1)_{kk}, \frac{1}{\lambda_k}(\boldsymbol{M}'_1)_{ll} \right\} = \left\{ \mathscr{I}'_{kk} + i\frac{2\pi a \varpi_k}{\cos \vartheta}, \mathscr{I}'_{ll} + i\frac{2\pi a \varpi_l}{\cos \vartheta} \right\}, \qquad (4.1)$$

where $\boldsymbol{M}'_1$ ((A 8) and (A 31)), λ_j ((A 25) and (A 10)), a (A 6) and Γ (A 36) are defined in the Appendix. The growth rates of the Floquet modes, in the asymptotic regime $\zeta \ll 1$, are equal to

$$\mathrm{Re}\,\sigma = \zeta \,\mathrm{Re}\,\Gamma / 2\pi; \qquad (4.2)$$

i.e. if $\mathrm{Re}\,\Gamma \neq 0$ we infer instability. Thus for $n \neq \pm 2$ the system remains stable, at least in the first order in ζ. The only possibility of destabilization in the first-order analysis appears for $n = \pm 2$. The frequencies of oscillation of the modes for $\zeta = 0$ are essentially the imaginary parts of the eigenvalues of $\boldsymbol{C}_0$ given in (A 10); hence

$$\begin{aligned}
\varpi_1 &= \cos \vartheta ((1 + \mathscr{R}_i) + \sqrt{(1 + \mathscr{R}_i)^2 + H^2}), \\
\varpi_2 &= -\cos \vartheta ((1 + \mathscr{R}_i) + \sqrt{(1 + \mathscr{R}_i)^2 + H^2}), \\
\varpi_3 &= \cos \vartheta ((1 + \mathscr{R}_i) - \sqrt{(1 + \mathscr{R}_i)^2 + H^2}), \\
\varpi_4 &= -\cos \vartheta ((1 + \mathscr{R}_i) - \sqrt{(1 + \mathscr{R}_i)^2 + H^2}).
\end{aligned} \qquad (4.3)$$

As Lebovitz & Zweibel (2004) already pointed out, the interchange $\cos \vartheta \to -\cos \vartheta$, i.e. the reversal of the direction of propagation along the z axis, leads to the same set of frequencies $\{\varpi_j\}$. Therefore, we may, without loss of generality, assume $\cos \vartheta > 0$. As a consequence, only the following four resonant cases need to be considered: $\varpi_1 - \varpi_2 = 2$, $\varpi_1 - \varpi_3 = 2$, $\varpi_1 - \varpi_4 = 2$ and $\varpi_4 - \varpi_3 = 2$.

Case 1 (*hydrodynamic resonance*): $\varpi_1 - \varpi_2 = 2$

The frequencies ϖ_1 and ϖ_2 correspond to hydrodynamic modes, modified by the presence of the magnetic field and the Coriolis force; in other words when $H \to 0$ they do not reduce to zero but asymptotically achieve the frequencies of modes from non-magnetic case (Miyazaki 1992). In the case at hand

$$\left\{ \begin{array}{l} \varpi_1 = -\varpi_2 \\ \varpi_1 - \varpi_2 = 2 \end{array} \right| \Rightarrow \quad \varpi_1 = 1, \quad \varpi_2 = -1; \qquad (4.4)$$

hence

$$\cos \vartheta = \frac{1}{(1 + \mathscr{R}_i) + \sqrt{(1 + \mathscr{R}_i)^2 + H^2}}, \qquad (4.5)$$

and since $\cos \vartheta \leqslant 1$,

$$H^2 \geqslant -2\mathscr{R}_i - 1 \qquad (4.6)$$

For $\mathscr{R}_i = H = 0$, i.e. for pure elliptical instability, $\cos \vartheta$ is $1/2$, so that $\vartheta = \pi/3$. When $H \to \infty$ or $\mathscr{R}_i \to \infty$, $\cos \vartheta$ tends to zero and $\vartheta \to \pi/2$. On the other hand, when $\mathscr{R}_i \to -\infty$, holding $H^2 \sim -2\mathscr{R}_i - 1$, $\cos \vartheta$ tends to 1 and ϑ to zero. The fact that $\varpi_1 = 1 = -\varpi_2$ in particular means a resonant coincidence of the frequencies ϖ_1 and ϖ_2 with the basic frequency ω.

By the use of (A 28), (A 31) and (A 40) we may obtain the Γ coefficient for this case,

$$\Gamma^2 = \frac{\pi^2}{4}(1 + \cos \vartheta)^4 - \pi^2 \left(\frac{2a}{\cos \vartheta} - \frac{(1 + \mathscr{R}_i) \cos \vartheta (1 - \cos^2 \vartheta)}{1 - (1 + \mathscr{R}_i) \cos \vartheta} \right)^2. \qquad (4.7)$$

Thus, with the aid of (4.2), the maximal growth rate achieved for

$$a = \frac{\cos^2 \vartheta \, (1 + \cos \vartheta)}{2} \frac{(1 + \mathscr{R}_i) (1 - \cos \vartheta)}{1 - (1 + \mathscr{R}_i) \cos \vartheta}$$

is

$$\sigma_{max} = \frac{\zeta \Gamma_{max}}{2\pi} = \frac{1}{4} \zeta (1 + \cos \vartheta)^2, \qquad (4.8)$$

and it depends on $\mathscr{R}_i$ and H via $\cos \vartheta$. For $H \to \infty$ or $\mathscr{R}_i \to \infty$, the maximal growth rate tends to the value $(1/4)\zeta$, dependent only on the ellipticity of the basic flow. It is worth mentioning that for $H^2 = -2\mathscr{R}_i - 1$, i.e. for the only case in which the horizontal instability is present for all values of δ, angle $\vartheta = 0$ for this resonance (which indicates that this mode becomes horizontal in this case).

Case 2 (*mixed resonance*): $\varpi_1 - \varpi_3 = 2$

This time the frequency ϖ_3 corresponds to a magnetic mode (i.e. when $H \to 0$ it reduces to zero), and ϖ_1, as previously, corresponds to a hydrodynamic mode. Now

$$\cos \vartheta = \frac{1}{\sqrt{(1 + \mathscr{R}_i)^2 + H^2}}, \qquad (4.9)$$

and hence

$$\varpi_1 = (1 + \mathscr{R}_i) \cos \vartheta + 1, \qquad \varpi_3 = (1 + \mathscr{R}_i) \cos \vartheta - 1. \qquad (4.10)$$

The condition $\cos \vartheta \leqslant 1$ results in

$$H^2 \geqslant -\mathscr{R}_i (\mathscr{R}_i + 2). \qquad (4.11)$$

For $\mathscr{R}_i = H = 0$ we have $\vartheta = 0$, and when $H \to \infty$ or $\mathscr{R}_i \to \pm\infty$, the angle $\vartheta \to \pi/2$. Also here, by the use of (A 28), (A 31) and (A 40) we calculate the coefficient Γ,

$$\Gamma = \mathrm{i}\pi (1 + \mathscr{R}_i) \cos \vartheta \left(\frac{2a}{\cos \vartheta} - 1 + \cos^2 \vartheta \right) \pm \sqrt{D}, \qquad (4.12)$$

where D given by Lebovitz & Zweibel (2004) for $\mathscr{R}_i = 0$ is now modified to

$$D = \pi^2 (1 - \cos^2 \vartheta)^2 [1 - (1 + \mathscr{R}_i)^2 \cos^2 \vartheta (3(1 + \mathscr{R}_i)^2 \cos^2 \vartheta + 2)]$$

$$+ 16\pi^2 \frac{a}{\cos^2 \vartheta} [(1 + \mathscr{R}_i)^2 \cos^3 \vartheta (1 - \cos^2 \vartheta) - a], \qquad (4.13)$$

which must be greater than zero in order to have instability. Now the maximal growth rate, which in this case is achieved for

$$a = \frac{\cos^3 \vartheta (1 - \cos^2 \vartheta)(1 + \mathscr{R}_i)^2}{2},$$

is

$$(\operatorname{Re}\sigma)_{max} = \frac{\zeta (\operatorname{Re}\Gamma)_{max}}{2\pi} = \frac{1}{4}\zeta (1 - \cos^2 \vartheta)(1 - (1 + \mathscr{R}_i)^2 \cos^2 \vartheta), \quad (4.14)$$

which, again, depends on $\mathscr{R}_i$ and H through $\cos \vartheta$. For $\mathscr{R}_i = H = 0$, when $\cos \vartheta = 1$, it is equal to 0, and when $H \to \infty$ or $\mathscr{R}_i \to \infty$, it tends, as previously, to $(1/4)\zeta$.

Case 3 (*magnetic resonance*): $\varpi_4 - \varpi_3 = 2$
In this case both frequencies correspond to magnetic modes not present when $H = 0$. This time

$$\left\{ \begin{array}{l} \varpi_4 = -\varpi_3 \\ \varpi_4 - \varpi_3 = 2 \end{array} \right| \Rightarrow \quad \varpi_4 = 1, \quad \varpi_3 = -1, \quad (4.15)$$

and the destabilized direction of propagation

$$\cos \vartheta = \frac{1}{\sqrt{(1 + \mathscr{R}_i)^2 + H^2} - (1 + \mathscr{R}_i)}. \quad (4.16)$$

Because $\cos \vartheta \leqslant 1$ this resonance type takes place only when

$$H^2 \geqslant 3 + 2\mathscr{R}_i. \quad (4.17)$$

Here, just as in case 1, the frequencies ϖ_3 and ϖ_4 are in resonance with the basic frequency ω. The coefficient Γ is now

$$\Gamma^2 = \frac{\pi^2}{4}(1 - \cos \vartheta)^4 - \pi^2 \left(\frac{2a}{\cos \vartheta} + \frac{(1 + \mathscr{R}_i)\cos \vartheta (1 - \cos^2 \vartheta)}{1 + (1 + \mathscr{R}_i)\cos \vartheta} \right)^2. \quad (4.18)$$

The maximal growth rate is achieved for

$$a = -\frac{\cos^2 \vartheta (1 - \cos \vartheta)}{2}\frac{(1 + \mathscr{R}_i)(1 + \cos \vartheta)}{1 + (1 + \mathscr{R}_i)\cos \vartheta}$$

and is equal to

$$\sigma_{max} = \frac{\zeta \Gamma_{max}}{2\pi} = \frac{1}{4}\zeta (1 - \cos \vartheta)^2. \quad (4.19)$$

For $H = \sqrt{3 + 2\mathscr{R}_i}$, when $\cos \vartheta = 1$, it is equal to zero, and when $H \to \infty$, the maximal growth rate tends, again, to $(1/4)\zeta$.

Case 4: $\varpi_1 - \varpi_4 = 2$
Like in case 2 the resonance here takes place between the hydrodynamic and magnetic modes. We get

$$\cos \vartheta = \frac{1}{1 + \mathscr{R}_i}, \quad (4.20)$$

and so

$$\varpi_1 = \sqrt{(1 + \mathscr{R}_i)^2 + H^2} \cos \vartheta + 1, \quad \varpi_4 = \sqrt{(1 + \mathscr{R}_i)^2 + H^2} \cos \vartheta - 1. \quad (4.21)$$

However, for such values of the frequencies, the matrix $\boldsymbol{J}'$, in accordance with (A 28), is diagonal. This means that the coefficient Γ is purely imaginary, and the system is stable (see (4.1)).
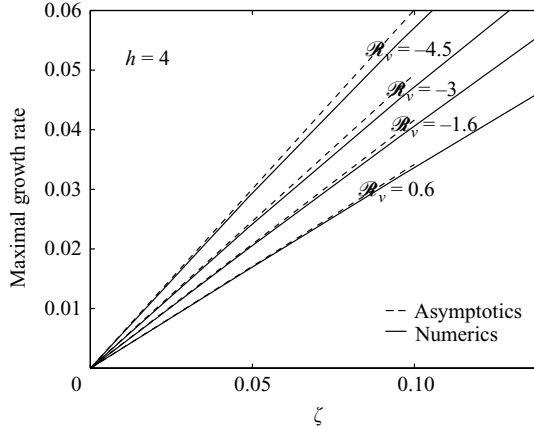
FIGURE 7. A comparison between the asymptotic theory and numerical solutions. The dependence of the maximal growth rate on the ellipticity ζ is shown for $h = 4$ and $\mathcal{R}_v = 0.6$, -1.6, -3, -4.5. The dashed straight lines are the theoretical predictions, and the continuous lines are obtained from numerical calculations.

The results of the asymptotic analysis performed in this section can explain some of the effects observed earlier in numerical solutions of the stability problem at hand, concerning the modes destabilized by the departure of the basic flow from axial symmetry. The magnetic field and the background rotation give rise to new unstable modes, destabilized by a resonant mechanism. The formulae (4.5), (4.9) and (4.16) obtained in the first-order analysis in the parameter ζ, i.e. for the thickest wedges, describe the directions along which the system is most likely to be destabilized and are in perfect agreement with numerical calculations. It also follows from these formulae that with increasing magnetic field strength or increasing background rotation, the directions of propagation of the unstable modes tend to the direction of the z axis, which was also observed in numerical solutions. This results in another effect, namely the decrease of growth rates of the modes destabilized via the resonant mechanism after switching on the magnetic field or the background rotation. The growth rate in the first case of resonance between two hydrodynamic modes, i.e. present also when $H = \mathcal{R}_i = 0$, has the highest value (see (4.8), (4.14) and (4.19)), and since switching on the magnetic field and the background rotation increases the angle ϑ associated with the unstable mode, it follows from (4.8) that the growth rate must then be decreased. Moreover, both formulae (4.5) and (4.8) suggest that for small ellipticities the dependence of the maximal growth rate on H should be monotonic. Hence, the minimum observed in figure 4 does not appear in this case. When $H \to \infty$ (or $\mathcal{R}_i \to \infty$) the growth rates given in (4.8), (4.14) and (4.19) tend to a value depending only on the ellipticity of the basic flow, $(1/4)\zeta$, in agreement with numerical predictions. We compare our asymptotic and numerical results in figure 7, where the dependence of the maximal growth rate on the ellipticity is presented for small values of ζ. The dashed lines are the straight lines predicted by our asymptotic theory, and the continuous lines are calculated numerically. We note that the asymptotic theory provides good agreement with the numerical calculations for ζ up to about 0.05.

Since the presence of the magnetic field introduces the dependence of the stability problem on the wavelength of the perturbations (through the parameter $H = k_0 B_0 / \sqrt{\mu_0 \rho} \omega$, which is proportional to the scale of the wave vector k_0), one more comment is necessary here. For a given magnetic field B_0 the formulae (4.8), (4.14) and (4.19) for the growth rates in the three resonant cases should also be maximized over

the parameter H. In case 1, that of the hydrodynamic resonance, the growth rate has a maximum at $H = 0$, and therefore the long wavelength perturbations are the most unstable. However, in cases 2 and 3, those of the mixed and magnetic resonances, the growth rates have a minimum at $H = 0$ and increase with H. It follows that short wavelength perturbations are preferable for these resonant cases.

4.1. *Finite vertical thickness and an upper bound for the magnetic field strength*

The idea of applying the results of the magnetoelliptic instability analysis to a system with finite vertical thickness d comes from Lebovitz & Zweibel (2004). It stems from the fact that the magnetoelliptic instability, as mentioned in the introduction, is likely to take place in accretion discs. Since in some cases the tidal deformation of the disc can rotate with a different angular velocity than the whole accretion disc, the incorporation of the Coriolis effect seems important. Here we would like to show how the resulting condition for the magnetic field strength at which this type of instability can operate is modified by the presence of the Coriolis force. If the vertical extent d of the system is finite, the z component of the wave vector of the perturbations cannot be smaller then C/d, where C the constant is a number of the order of unity. When $\mathscr{R}_i \geqslant -1$ all three above-mentioned resonant cases which lead to instability, i.e. (4.5) and (4.6), (4.9) and (4.11) and (4.16) and (4.17), imply $H \cos \vartheta \leqslant \sqrt{3 + 2\mathscr{R}_i}$. Thus the condition that must be satisfied in order for the elliptical instability to operate takes the form

$$
\begin{cases} k_0 \cos \vartheta \leqslant \sqrt{3 + 2\mathscr{R}_i} \, \dfrac{\omega}{u_A} \\ k_0 \cos \vartheta \geqslant \dfrac{C}{d} \end{cases} \Rightarrow u_A \leqslant \sqrt{3 + 2\mathscr{R}_i} \dfrac{\omega d}{C} \quad \text{and} \quad \mathscr{R}_i \geqslant -1 \;, \quad (4.22)
$$

where $u_A = B_0 / \sqrt{\mu_0 \rho}$ is the Alfvén speed. Analogously, when $\mathscr{R}_i < -1$ the same set of equations implies $H \cos \vartheta \leqslant \sqrt{-2\mathscr{R}_i - 1}$, and hence

$$
\begin{cases} k_0 \cos \vartheta \leqslant \sqrt{-2\mathscr{R}_i - 1} \, \dfrac{\omega}{u_A} \\ k_0 \cos \vartheta \geqslant \dfrac{C}{d} \end{cases} \Rightarrow u_A \leqslant \sqrt{-2\mathscr{R}_i - 1} \dfrac{\omega d}{C} \quad \text{and} \quad \mathscr{R}_i < -1. \quad (4.23)
$$

Thus, the presence of the Coriolis force significantly modifies the conditions at which the elliptical instability is possible in an accretion disc of thickness d. In most cases, i.e. for cyclonic rotation, and anticyclonic if $\mathscr{R}_i < -2$ the bound on B_0 is eased by the presence of background rotation.

However, as mentioned in the introduction, our results are most likely to apply to an elliptical vortex patch embedded in the accretion disc, created by the non-uniform average angular velocity profile in the disc rather than the whole disc itself, since in the latter case the effects of differential rotation are likely to predominate.

5. Conclusions

We have analysed here the problem of elliptical instability in the presence of background rotation and external magnetic field. Our motivation comes mainly from possible astrophysical applications, i.e. the investigation of the influence of tidal deformations of astrophysical objects such as planet cores, stars and accretion discs on their global stability characteristics. Here, we have investigated the joint effect on such systems of the Lorentz and Coriolis forces, the two factors which play a crucial role in the dynamics of the fluid interiors of such objects. Apart from accretion discs, for which we have derived the formulae (4.22) and (4.23), the case of Io and

Ganymede, Jupiter's moons, is particularly interesting, since large tidal deformations on these satellites caused by Jupiter are very likely to trigger instability (Kerswell & Malkus 1998; Lacaze *et al.* 2006). Moreover, Mizerski *et al.* (2009) have argued that the elliptical instability is capable of generating magnetic field, and since the convective dynamo mechanism is very unlikely now on such small bodies as Io and Ganymede, the elliptical instability is a promising mechanism of generation of their magnetic fields (Lacaze *et al.* 2006). Generally, in all tidally deformed astrophysical objects, where the flow of rapidly rotating conducting fluid is considered, the influence of the magnetic field and the background rotation on their stability characteristics is crucial and non-trivial. Although the effect that these factors exert in isolation has already been studied (Miyazaki 1993; Lebovitz & Zweibel 2004) this is, as far as we know, the first detailed investigation of their joint effect on the stability problem of elliptical flow.

In §4 and in the Appendix, we have used the asymptotic technique of Lebovitz & Zweibel (2004) for small ellipticities of the basic flow to establish the growth rates of the unstable perturbations and their directions of propagation. (In other words we have determined the directions along which the system is most likely to be destabilized when it slightly departs from axial symmetry.) These results are in perfect agreement with the numerical analysis of the stability problem, which we have also performed and which allowed for a detailed investigation of the influence of the background rotation and the magnetic field on elliptical instability. We have analysed the growth rates for a wide range of values of all the parameters in the system. The dependence of the growth rates on the magnetic field strength h, the intensity of the background rotation $\mathcal{R}_v$ and the strain parameter $0 < \epsilon < 1$ (which can be regarded as a measure of ellipticity of the basic flow) was computed. We have also obtained the directions of propagation of the unstable modes and their growth rates for varying ellipticity δ.

The influence of the Lorentz and Coriolis forces on the elliptical instability turns out to be quite complex. In the absence of horizontal instability (Bajer & Mizerski 2009), i.e. for $\mathcal{R}_v > -h^2/4$, both these factors exert a stabilizing effect, by decreasing the growth rates and the range of directions of propagation of the unstable perturbations. On the other hand the presence of the magnetic field and the background rotation allow for much more destabilizing resonances between the frequencies of oscillation of the perturbations or in other words larger variety of unstable modes. This effect is most clearly seen when both these factors are present at once. Additionally the joint action of the Lorentz and Coriolis forces very effectively enlarges the range of existence of the horizontal instability. This type of instability, which is not of resonant nature, is mainly characterized by large growth rates and a wide range of directions of propagation of unstable modes and is present only for anticyclonic rotation $\mathcal{R}_v = \gamma/\Omega < 0$, exhibits a singular behaviour when the external magnetic field decreases to zero. When $h = 0$ it exists only within a bounded interval $-1 < \mathcal{R}_v < 0$, but when the magnetic field is switched on, the range of values of parameter $\mathcal{R}_v$ at which horizontal instability is present becomes unbounded from below, $\mathcal{R}_v < -h^2/4$. In contrast with all other unstable modes excited via a resonant mechanism the horizontal instability is not suppressed in the limit of large ellipticity of the basic flow, when $\epsilon \to 1$, and the basic flow becomes the pure shear flow.

An important conclusion of the analysis performed is that the systems with anticyclonic rotation that are in the range of existence of horizontal instability, i.e. for $\mathcal{R}_v < -h^2/4$, are more likely to develop turbulence, since the dissipative effects are less likely to damp the instability. Another interesting observation is that in the limit of strong magnetic field (or rapid rotation), the maximal growth rates depend only on the ellipticity of the basic flow, and in the asymptotic limit, when this ellipticity is small, they are equal to $\mathrm{Re}\,(\sigma)_{max} = \epsilon/4\sqrt{1 - \epsilon^2}$.

In §3 we have presented the time evolution of a selected unstable mode, by visualizing the evolution of the streamlines, magnetic field lines and the lines of electric currents and also of the trajectories of a selected fluid particle.

We conclude by stating that the joint effect of the Coriolis and Lorentz forces is qualitatively and quantitatively different from the effect they exert in isolation. The analysis of their joint influence on the elliptical instability has revealed interesting and new characteristics of the problem. It is important to keep in mind, however, that in the astrophysical context of stellar and planetary interiors, thermal phenomena are a fundamental factor in the dynamics and must be taken into account. The results of Le Bars & Le Dizes (2006) suggest that the thermal phenomena may, in some cases, suppress the elliptical instability.

Appendix. Small ellipticity asymptotics

Here we use the asymptotic method of Lebovitz & Zweibel (2004) to calculate growth rates of the modes destabilized by small departure of the basic flow from axial symmetry, $\zeta = (1/2)(E - E^{-1}) \ll 1$. First we introduce new variables:

$$\left.\begin{aligned}
c_1 &= E k_x v_y - E^{-1} k_y v_x, \\
c_2 &= k_x v_x + k_y v_y, \\
c_3 &= E k_x b_y - E^{-1} k_y b_x, \\
c_4 &= k_x b_x + k_y b_y.
\end{aligned}\right\} \tag{A 1}$$

We observe that such transformation is periodic in time and therefore does not affect the stability problem. Equation (2.24) is now

$$\frac{\mathrm{d}c}{\mathrm{d}\tau} = \mathbf{C}(\tau)\,c, \tag{A 2}$$

where the only non-zero elements of $\mathbf{C}(\tau)$ are

$$\left.\begin{aligned}
\mathscr{C}_{11} &= \frac{4k_x k_y}{k^2}\zeta\left(\mathscr{R}_i \frac{k_z^2}{E k_x^2 + E^{-1}k_y^2} - 1\right), \\
\mathscr{C}_{12} &= -2\left(1 + \mathscr{R}_i \frac{E^2 k_x^2 + E^{-2}k_y^2}{E k_x^2 + E^{-1}k_y^2} - 4\mathscr{R}_i\zeta^2 \frac{k_x^2 k_y^2}{k^2\left(E k_x^2 + E^{-1}k_y^2\right)}\right), \\
\mathscr{C}_{13} &= \mathrm{i}H\cos\vartheta, \\
\mathscr{C}_{21} &= \frac{2k_z^2}{k^2}\left(1 + \mathscr{R}_i \frac{k_x^2 + k_y^2}{E k_x^2 + E^{-1}k_y^2}\right), \\
\mathscr{C}_{22} &= -4\mathscr{R}_i\zeta \frac{k_x k_y k_z^2}{k^2\left(E k_x^2 + E^{-1}k_y^2\right)}, \\
\mathscr{C}_{24} &= \mathscr{C}_{31} = \mathscr{C}_{42} = \mathrm{i}H\cos\vartheta.
\end{aligned}\right\} \tag{A 3}$$

The matrix $\mathbf{C}(\tau)$ is periodic in τ, and therefore (A 2), just as (2.24), constitutes a Floquet problem. The important difference, however, is that for $\zeta = 0$ ($E = 1$) matrix

C, unlike S, is independent of τ,

$$
C\left(\zeta=0\right)\doteq C_0=\begin{bmatrix} 0 & -2\left(1+\mathscr{R}_i\right)\mathrm{i}H\cos\vartheta & 0 \\ \frac{2k_z^2}{k_0^2}\left(1+\mathscr{R}_i\right) & 0 & 0 & \mathrm{i}H\cos\vartheta \\ \mathrm{i}H\cos\vartheta & 0 & 0 & 0 \\ 0 & \mathrm{i}H\cos\vartheta & 0 & 0 \end{bmatrix}. \quad (A\,4)
$$

The fundamental solution of this equation we will denote by $\mathscr{M}\left(\tau\right)$. All the conclusions concerning the matrix $M\left(2\pi\right)$ stated in §4 are also true for $\mathscr{M}\left(2\pi\right)$, which for brevity will be denoted as $\widehat{\mathbb{M}}$.

We expand $\widehat{\mathbb{M}}$ in Taylor series around $\zeta=0$ and $\cos\vartheta=\cos\vartheta_0$, for some wedge apex $(0,\vartheta_0)$, holding H and $\mathscr{R}_i$ constant,

$$
\widehat{\mathbb{M}}\left(\zeta,\cos\vartheta\right)=\widehat{\mathbb{M}}\left(0,\cos\vartheta_0\right)+\zeta\frac{\partial\widehat{\mathbb{M}}}{\partial\zeta}\left(0,\cos\vartheta_0\right)
$$

$$
+\left(\cos\vartheta-\cos\vartheta_0\right)\frac{\partial\widehat{\mathbb{M}}}{\partial\left(\cos\vartheta\right)}\left(0,\cos\vartheta_0\right)+O(\zeta^2,\left(\cos\vartheta-\cos\vartheta_0\right)^2). \quad (A\,5)
$$

The direction of propagation of a mode may also change when it becomes unstable, and therefore

$$
\cos\vartheta=\cos\vartheta_0+a\zeta+O(\zeta^2). \quad (A\,6)
$$

This in fact means that we are including only the thickest wedges, whose thickness is of order ζ in our analysis. (To include also the thinner wedges we would have to go to higher orders.) Equation (A 5) may now be written as

$$
\widehat{\mathbb{M}}=\widehat{\mathbb{M}}_0+\zeta\widehat{\mathbb{M}}_1+O(\zeta^2), \quad (A\,7)
$$

where

$$
\widehat{\mathbb{M}}_0=\widehat{\mathbb{M}}\left(0,\cos\vartheta_0\right) \quad \widehat{\mathbb{M}}_1=\frac{\partial\widehat{\mathbb{M}}}{\partial\zeta}\left(0,\cos\vartheta_0\right)+a\frac{\partial\widehat{\mathbb{M}}}{\partial\left(\cos\vartheta\right)}\left(0,\cos\vartheta_0\right). \quad (A\,8)
$$

A.1. *Matrices* $\widehat{\mathbb{M}}_0$ *and* $\widehat{\mathbb{M}}_1$

We will now proceed to calculate the matrices $\widehat{\mathbb{M}}_0$ and $\widehat{\mathbb{M}}_1$. Let us write the expansion of $C\left(\tau\right)$ in Taylor series around $\zeta=0$ at fixed $\cos\vartheta$,

$$
C\left(\tau,\zeta,\cos\vartheta\right)=C_0\left(\tau,\cos\vartheta\right)+\zeta\frac{\partial C}{\partial\zeta}\left(\tau,\cos\vartheta\right)+O(\zeta^2). \quad (A\,9)
$$

Operator C_0 is given in (A 4), and since it does not depend on time we may calculate its eigenvalues,

$$
\left.\begin{aligned} s_1&=\mathrm{i}\cos\vartheta((1+\mathscr{R}_i)+\sqrt{(1+\mathscr{R}_i)^2+H^2}),\\ s_2&=-\mathrm{i}\cos\vartheta((1+\mathscr{R}_i)+\sqrt{(1+\mathscr{R}_i)^2+H^2}),\\ s_3&=\mathrm{i}\cos\vartheta((1+\mathscr{R}_i)-\sqrt{(1+\mathscr{R}_i)^2+H^2}),\\ s_4&=-\mathrm{i}\cos\vartheta((1+\mathscr{R}_i)-\sqrt{(1+\mathscr{R}_i)^2+H^2}), \end{aligned}\right\} \quad (A\,10)
$$

which are the zeroth-order approximation of the growth rates. We assume now $\cos\vartheta\neq0$ and $H\neq0$ so that these eigenvalues are distinct and non-zero. The matrix $\left(\partial C/\partial\zeta\right)\left(\tau,\cos\vartheta\right)$ can easily be calculated from (A 9), and its only non-zero elements

are

$$\left(\frac{\partial \mathbf{C}}{\partial \zeta}\right)_{11} = i(e^{2i\tau} - e^{-2i\tau})[1 - (1 + \mathscr{R}_i)\cos^2 \vartheta],$$

$$\left(\frac{\partial \mathbf{C}}{\partial \zeta}\right)_{12} = -\mathscr{R}_i(e^{2i\tau} + e^{-2i\tau}),$$

$$\left(\frac{\partial \mathbf{C}}{\partial \zeta}\right)_{21} = \cos^2 \vartheta[1 - (1 + \mathscr{R}_i)\cos^2 \vartheta](e^{2i\tau} + e^{-2i\tau}) - 2\cos^2 \vartheta[1 - \cos^2 \vartheta](1 + \mathscr{R}_i),$$

$$\left(\frac{\partial \mathbf{C}}{\partial \zeta}\right)_{22} = i\mathscr{R}_i \cos^2 \vartheta(e^{2i\tau} - e^{-2i\tau}).$$

$$(A\,11)$$

We may now construct the matrices $\widehat{\mathbf{M}}_0 (\cos \vartheta)$ and $(\partial \widehat{\mathbf{M}}/\partial \zeta)(\cos \vartheta)$. The former is simply

$$\widehat{\mathbf{M}}_0 = \exp(2\pi \mathbf{C}_0). \tag{A\,12}$$

Next, for a given $\tau \in [0, 2\pi]$ and $\cos \vartheta$ we expand

$$\mathscr{M}(\tau, \zeta, \cos \vartheta) = \mathscr{M}_0(\tau, \cos \vartheta) + \zeta \mathscr{M}_1(\tau, \cos \vartheta) + O(\zeta^2), \tag{A\,13}$$

and substituting this form in (A 2), with the aid of (A 9), we obtain

$$\frac{\mathrm{d}\mathscr{M}_0}{\mathrm{d}\tau} = \mathbf{C}_0 \mathscr{M}_0, \tag{A\,14}$$

$$\frac{\mathrm{d}\mathscr{M}_1}{\mathrm{d}\tau} = \mathbf{C}_0 \mathscr{M}_1 + \frac{\partial \mathbf{C}}{\partial \zeta} \mathscr{M}_0, \tag{A\,15}$$

with initial conditions (see (2.29))

$$\mathscr{M}_0(\tau = 0) = \mathbf{I} \qquad \mathscr{M}_1(\tau = 0) = \widehat{0}. \tag{A\,16}$$

The solution of (A 14) is

$$\mathscr{M}_0 = \exp(\mathbf{C}_0 \tau), \tag{A\,17}$$

whereas of (A 15) at $\tau = 2\pi$ is

$$\mathscr{M}_1(2\pi) = \frac{\partial \widehat{\mathbf{M}}}{\partial \zeta}(\cos \vartheta) = \widehat{\mathbf{M}}_0(\cos \vartheta) \int_0^{2\pi} \mathscr{M}_0^{-1}(\tau, \cos \vartheta) \frac{\partial \mathbf{C}}{\partial \zeta}(\tau, \cos \vartheta) \mathscr{M}_0(\tau, \cos \vartheta) \,\mathrm{d}\tau. \tag{A\,18}$$

The aim of this calculation is to obtain the growth rates of the perturbations, hence the eigenvalues of $\widehat{\mathbf{M}}$ (see (2.30)), which do not depend on the choice of the coordinate system. To simplify the calculation we will now express all the variables in the base diagonalizing $\mathbf{C}_0$,

$$\mathbf{C}_0' = \widehat{T}^{-1} \mathbf{C}_0 \widehat{T} = \mathrm{diag}(s_1, s_2, s_3, s_4), \tag{A\,19}$$

where the columns of $\widehat{T}$ are the eigenvectors of $\mathbf{C}_0$ expressed in the old base, i.e.

$$\widehat{T} = \begin{bmatrix} s_1 & s_2 & s_3 & s_4 \\ -i\cos \vartheta\, s_1 & i\cos \vartheta\, s_2 & -i\cos \vartheta\, s_3 & i\cos \vartheta\, s_4 \\ iH \cos \vartheta & iH \cos \vartheta & iH \cos \vartheta & iH \cos \vartheta \\ H \cos^2 \vartheta & -H \cos^2 \vartheta & H \cos^2 \vartheta & -H \cos^2 \vartheta \end{bmatrix} \tag{A\,20}$$

and

$$
\widehat{T}^{-1} = \frac{1}{\Delta}
\begin{bmatrix}
-\mathrm{i}H\cos\vartheta & H & s_3 & \frac{\mathrm{i}s_3}{\cos\vartheta} \\
\mathrm{i}H\cos\vartheta & H & s_3 & -\frac{\mathrm{i}s_3}{\cos\vartheta} \\
\mathrm{i}H\cos\vartheta & -H & -s_1 & -\frac{\mathrm{i}s_1}{\cos\vartheta} \\
-\mathrm{i}H\cos\vartheta & -H & -s_1 & \frac{\mathrm{i}s_1}{\cos\vartheta}
\end{bmatrix},
\tag{A 21}
$$

with $\Delta = 4H\cos^2\vartheta\sqrt{(1+\mathcal{R}_i)^2 + H^2}$. Thus in the new base

$$
\frac{\partial\widehat{\mathbb{M}'}}{\partial\zeta}(\cos\vartheta) = \widehat{\mathbb{M}'_0}(\cos\vartheta)\,\boldsymbol{J}'(\cos\vartheta),
\tag{A 22}
$$

where

$$
\boldsymbol{J}'(\cos\vartheta) = \int_0^{2\pi} \mathcal{M}'^{-1}_0(\tau,\cos\vartheta)\,\frac{\partial\boldsymbol{C}'}{\partial\zeta}(\tau,\cos\vartheta)\,\mathcal{M}'_0(\tau,\cos\vartheta)\,\mathrm{d}\tau
\tag{A 23}
$$

and $'$ indicates that the operator is expressed in the base of eigenvectors of $\boldsymbol{C}_0$. since s_i, $i = 1, 2, 3, 4$, are distinct, the matrix $\mathcal{M}'_0$ given in (A 17) and $\widehat{\mathbb{M}'_0}$ are diagonal,

$$
\mathcal{M}'_0 = \mathrm{diag}(\exp(s_1\tau), \exp(s_2\tau), \exp(s_3\tau), \exp(s_4\tau)),
\tag{A 24}
$$

$$
\widehat{\mathbb{M}'_0} = \mathrm{diag}(\lambda_1, \lambda_2, \lambda_3, \lambda_4) \quad \text{where} \quad \lambda_i = \exp(2\pi s_i), \quad \text{for} \quad i = 1, 2, 3, 4. \tag{A 25}
$$

The matrix $(\partial\boldsymbol{C}/\partial\zeta)(\tau,\cos\vartheta)$ has only four non-zero elements (A 11); hence

$$
\mathcal{I}'_{ij} = T^{-1}_{i1}T_{1j}\int_0^{2\pi} \mathrm{e}^{(s_j-s_i)\tau}\left(\frac{\partial\boldsymbol{C}}{\partial\zeta}\right)_{11}(\tau)\,\mathrm{d}\tau + T^{-1}_{i2}T_{1j}\int_0^{2\pi} \mathrm{e}^{(s_j-s_i)\tau}\left(\frac{\partial\boldsymbol{C}}{\partial\zeta}\right)_{21}(\tau)\,\mathrm{d}\tau
$$
$$
+ T^{-1}_{i1}T_{2j}\int_0^{2\pi} \mathrm{e}^{(s_j-s_i)\tau}\left(\frac{\partial\boldsymbol{C}}{\partial\zeta}\right)_{12}(\tau)\,\mathrm{d}\tau + T^{-1}_{i2}T_{2j}\int_0^{2\pi} \mathrm{e}^{(s_j-s_i)\tau}\left(\frac{\partial\boldsymbol{C}}{\partial\zeta}\right)_{22}(\tau)\,\mathrm{d}\tau, \tag{A 26}
$$

which allows us to calculate $(\partial\widehat{\mathbb{M}'}/\partial\zeta)(\cos\vartheta)$. Let us remind that the destabilization of the system, as pointed out in §4, occurs through a resonance between at least two eigenvalues of the matrix $\widehat{\mathbb{M}}$, and as in Lebovitz & Zweibel 2004, only the case of double multiplicity of the eigenvalue will be considered here. (Though higher multiplicities are, in general, possible.) Because the eigenvalues of the zeroth-order matrix $\widehat{\mathbb{M}}_0$ are of the form $\lambda_j = \exp(2\pi s_j)$, $j = 1, 2, 3, 4$, destabilization occurs for $s_i - s_j = \mathrm{i}k$, where $k \in \mathbb{N}\setminus\{0\}$ and zero is excluded because $\{s_j\}$ are distinct. Moreover with the aid of (A 11) we deduce that the diagonal elements of the matrix $\mathcal{I}'_{ij}$ (A 26) are non-zero, but the off-diagonal ones are non-zero only when $s_i - s_j = \pm 2\mathrm{i}$. Below we give the full list of the elements of $\mathcal{I}'_{ij}$ which we will need in the following analysis, for $s_i - s_j = +2\mathrm{i}$.

Diagonal elements:

$$\mathscr{I}'_{11} = -\mathrm{i}\pi\varpi_1 \frac{4H\cos^2\vartheta}{\Delta}(1+\mathscr{R}_i)(1-\cos^2\vartheta),$$

$$\mathscr{I}'_{22} = -\mathrm{i}\pi\varpi_2 \frac{4H\cos^2\vartheta}{\Delta}(1+\mathscr{R}_i)(1-\cos^2\vartheta),$$

$$\mathscr{I}'_{33} = \mathrm{i}\pi\varpi_3 \frac{4H\cos^2\vartheta}{\Delta}(1+\mathscr{R}_i)(1-\cos^2\vartheta),$$

$$\mathscr{I}'_{44} = \mathrm{i}\pi\varpi_4 \frac{4H\cos^2\vartheta}{\Delta}(1+\mathscr{R}_i)(1-\cos^2\vartheta).$$

(A 27)

Off-diagonal elements:

$$\left.\begin{array}{c}\mathscr{I}'_{12} = \mathrm{i}\tfrac{1}{2}\pi\varpi_2\,(1+\cos\vartheta)^2 \\ \mathscr{I}'_{21} = \mathrm{i}\tfrac{1}{2}\pi\varpi_1\,(1+\cos\vartheta)^2\end{array}\right\} \quad \text{for} \quad \varpi_1 - \varpi_2 = 2,$$

$$\left.\begin{array}{c}\mathscr{I}'_{13} = \mathrm{i}\tfrac{1}{2}\pi\varpi_3(1-\cos^2\vartheta)(1+(1+\mathscr{R}_i)\cos\vartheta) \\ \mathscr{I}'_{31} = \mathrm{i}\tfrac{1}{2}\pi\varpi_1(1-\cos^2\vartheta)(1-(1+\mathscr{R}_i)\cos\vartheta)\end{array}\right\} \quad \text{for} \quad \varpi_1 - \varpi_3 = 2,$$

$$\left.\begin{array}{c}\mathscr{I}'_{41} = 0 \\ \mathscr{I}'_{14} = 0\end{array}\right\} \quad \text{for} \quad \varpi_4 - \varpi_1 = 2,$$

$$\left.\begin{array}{c}\mathscr{I}'_{34} = \mathrm{i}\tfrac{1}{2}\pi\varpi_4\,(1-\cos\vartheta)^2 \\ \mathscr{I}'_{43} = \mathrm{i}\tfrac{1}{2}\pi\varpi_3\,(1-\cos\vartheta)^2\end{array}\right\} \quad \text{for} \quad \varpi_3 - \varpi_4 = 2,$$

(A 28)

where

$$s_j = \mathrm{i}\varpi_j \quad \text{for} \quad j = 1, 2, 3, 4. \tag{A 29}$$

We only need now the derivative $(\partial\widehat{\mathbf{M}}'/\partial(\cos\vartheta))(\cos\vartheta)$, which appears in (A 7) and (A 8). By the use of (A 25) and (A 10),

$$\frac{\partial\widehat{\mathbf{M}}'}{\partial(\cos\vartheta)}(\cos\vartheta) = \mathrm{diag}\left(\lambda_1\frac{2\pi s_1}{\cos\vartheta}, \lambda_2\frac{2\pi s_2}{\cos\vartheta}, \lambda_3\frac{2\pi s_3}{\cos\vartheta}, \lambda_4\frac{2\pi s_4}{\cos\vartheta}\right), \tag{A 30}$$

and thus finally (A 7), (A 8), (A 25), (A 27), (A 28) and (A 30) allow for calculation of $\widehat{\mathbf{M}}'_1 = \widehat{\mathbf{M}}'_0\mathbf{J}' + a(\partial\widehat{\mathbf{M}}'/\partial(\cos\vartheta))$,

$$(\widehat{\mathbf{M}}'_1)_{jj} = \lambda_j\left(\mathscr{I}'_{jj} + \mathrm{i}\frac{2\pi a\varpi_j}{\cos\vartheta}\right),$$

$$(\widehat{\mathbf{M}}'_1)_{jk} = \lambda_j\mathscr{I}'_{jk} \quad \text{where} \quad k \neq j, \tag{A 31}$$

where no summation is taken over j.

A.2. *Characteristic polynomial*

Further analysis of the characteristic polynomial of $\widehat{\mathbf{M}}$ leading to quadratic equation for the first-order correction to the growth rate is of general nature and is exactly the same as in Lebovitz & Zweibel (2004). We will therefore only briefly review the necessary steps and write down the resulting equation. We expand the characteristic polynomial of $\widehat{\mathbf{M}}$,

$$w(\lambda, \zeta) = \det(\widehat{\mathbf{M}}(\zeta) - \Lambda\mathbf{I}) = 0, \tag{A 32}$$

in perturbative series around $\zeta = 0$ to second order in ζ,

$$w(\lambda, \zeta) = w_0(\lambda) + \zeta w_1(\lambda) + \zeta^2 w_2(\lambda) + O(\zeta^3), \tag{A 33}$$

where $w_0(\lambda)$ is the characteristic polynomial of $\widehat{\mathbf{M}}_0$, the roots of which $\lambda_j = \exp(2\pi\sigma_j)$, $j = 1, 2, 3, 4$, are already known. The condition for destabilization is that there exist

multiple eigenvalues Λ_j, i.e multiple roots of $w(\lambda, \zeta)$. The Puiseux method, which is basically a variation of the implicit function theorem (Hille 1962) determines the character of expansion of the eigenvalues Λ_j, which depends on their multiplicity when $\zeta = 0$, i.e. the multiplicity of λ_j. Since we only consider the case in which the eigenvalues are multiplicity 2, the expansion takes the form

$$\Lambda_1(\zeta) = \lambda_1 + \zeta^{\frac{1}{2}}\beta_{1/2} + \zeta\beta_1 + O(\zeta^{\frac{3}{2}}), \tag{A 34}$$

where, for definiteness, we have assumed that $\lambda_1 = \lambda_2$. It can be shown, however, that $\beta_{1/2} = 0$ in this case, and then the leading-order correction to the eigenvalue, $\beta_1 \neq 0$, can be established from a quadratic equation,

$$\frac{1}{2}\frac{\mathrm{d}^2 w_0}{\mathrm{d}\lambda^2}(\lambda_1)\beta_1^2 + \frac{\mathrm{d}w_1}{\mathrm{d}\lambda}(\lambda_1)\beta_1 + w_2(\lambda_1) = 0. \tag{A 35}$$

Defining

$$\Gamma = \frac{\beta_1}{\lambda_1} \tag{A 36}$$

and with the aid of (A 34) we get $|\Lambda_1| = \sqrt{(1 + \zeta\,\mathrm{Re}\Gamma)^2 + (\zeta\,\mathrm{Im}\Gamma)^2} = 1 + \zeta\,\mathrm{Re}\Gamma + O(\zeta^2)$, and since $\mathrm{e}^{2\pi\sigma} = \Lambda$, the growth rate $\mathrm{Re}\sigma = \zeta\,\mathrm{Re}\Gamma/2\pi + O(\zeta^2)$. This means that the system is unstable only if $\mathrm{Re}\Gamma \neq 0$.

Now, by the use of the formulae for the derivatives of the characteristic polynomial with respect to parameter ζ, derived by Lebovitz & Zweibel (2004), we may calculate the coefficients $(\mathrm{d}^2 w_0/\mathrm{d}\lambda^2)(\lambda_1)$, $(\mathrm{d}w_1/\mathrm{d}\lambda)(\lambda_1)$ and $w_2(\lambda_1)$ from (A 35),

$$\frac{\mathrm{d}^2 w_0}{\mathrm{d}\lambda^2}(\lambda_1) = 2(\lambda_3 - \lambda_1)(\lambda_4 - \lambda_1), \tag{A 37}$$

$$\frac{\mathrm{d}w_1}{\mathrm{d}\lambda}(\lambda_1) = -\big[(\widehat{\mathbb{M}}'_1)_{11} + (\widehat{\mathbb{M}}'_1)_{22}\big](\lambda_3 - \lambda_1)(\lambda_4 - \lambda_1), \tag{A 38}$$

$$w_2(\lambda_1) = \det\begin{pmatrix}(\widehat{\mathbb{M}}'_1)_{11} & (\widehat{\mathbb{M}}'_1)_{12} \\ (\widehat{\mathbb{M}}'_1)_{21} & (\widehat{\mathbb{M}}'_1)_{22}\end{pmatrix}(\lambda_3 - \lambda_1)(\lambda_4 - \lambda_1). \tag{A 39}$$

Going back now to the general case of $\lambda_l = \lambda_k$, the quadratic equation (A 35), with the aid of (A 31), can easily be transformed to an equation for the coefficient $\Gamma = \beta_1/\lambda_k$,

$$\Gamma^2 - \left[\frac{1}{\lambda_k}(\widehat{\mathbb{M}}'_1)_{kk} + \frac{1}{\lambda_k}(\widehat{\mathbb{M}}'_1)_{ll}\right]\Gamma + \det\begin{pmatrix}\dfrac{1}{\lambda_k}(\widehat{\mathbb{M}}'_1)_{kk} & \mathscr{I}'_{kl} \\[2mm] \mathscr{I}'_{lk} & \dfrac{1}{\lambda_k}(\widehat{\mathbb{M}}'_1)_{ll}\end{pmatrix} = 0. \tag{A 40}$$

REFERENCES

ALDRIDGE, K. D. & LUMB, L. I. 1987 Inertial waves identified in the Earth's fluid outer core. *Nature* **325**, 421–423.

BAJER, K. & MIZERSKI, K. A. 2009 Elliptical flow instability triggered by a magnetic field. *Phys. Rev. Lett.* Submitted.

BALBUS, S. A. & HAWLEY, J. F. 1991 A powerful local shear instability in weakly magnetized disks. Part 1. Linear analysis. *Astrophys. J.* **376**, 214–222.

BAYLY, B. J. 1986 Three-Dimensional instability of elliptical flow. *Phys. Rev. Lett.* **57** (17), 2160–2163.

BRAGINSKY, S. I. 1991 Towards a realistic theory of the geodynamo. *Geophys. Astrophys. Fluid Dyn.* **60**, 89–134.

BRAGINSKY, S. I. 1999 Dynamics of the stably stratified ocean at the top of the core. *Phys. Earth Planet. Inter.* **111**, 21–34.

CADOT, O., DOUADY, S. & COUDER, Y. 1995 Characterization of the low pressure filaments in three-dimensional turbulent shear flow. *Phys. Fluids* **7**, 630.

CHANDRASEKHAR, S. 1969 *Ellipsoidal Figures of Equilibrium*, Yale University Press.

CRAIK, A. D. D. 1986 Exact solutions of non-conservative equations for three-wave and second-harmonic resonance. *Proc. R. Soc. Lond.* A **406**, 1–12.

CRAIK, A. D. D. 1988 A class of exact solutions in viscous incompressible magnetohydrodynamics. *Proc. R. Soc. Lond.* A **417**, 235–244.

CRAIK, A. D. D. 1989 The stability of unbounded two- and three-dimensional flows subject to body forces: some exact solutions. *J. Fluid Mech.* **198**, 275–292.

CRAIK, A. D. D. & CRIMINALE, W. O. 1986 Evolution of wave-like disturbances in shear flows. A class of exact-solutions of the Navier–Stokes equations. *Proc. R. Soc. Lond.* A **406**, 13–26.

CROSSLEY, D. J., HINDERER, J. & LEGROS, H. 1991 On the excitation, detection and damping of core modes. *Phys. Earth Plant. Inter.* **68**, 97–116.

ELOY, C H., LE GAL, P. & LE DIZÈS, S. 2000 Experimental study of the multipolar vortex instability. *Phys. Rev. Lett.* **85**, 3400–3403.

FABRE, D. & JACQUIN, L. 2004 Short-wave cooperative instabilities in representative aircraft vortices. *Phys. Fluids* **16**, 1366.

GOODMAN, J. 1993 The local instability of tidally distorted accretion disks. *Astrophys. J.* **406**, 596–613.

HASEGAWA, H. 2005 Structure of the magnetopause boundary layers discovered by Cluster multipoint observations. In *Proceedings of the Cluster and Double Star Symposium: Fifth Anniversary of Cluster in Space*, Noordwijk, Denmark.

HILLE, E. 1962 *Analytic Function Theory*, vol. 2. Ginn.

JI, H., BURIN, M., SCHARTMAN, E. & GOODMAN, J. 2006 Hydrodynamic turbulence cannot transport angular momentum effectively in astrophysical disks. *Nature* **444**, 343–346. Doi:10.1038/nature05323.

KELVIN, LORD W. THOMSON 1887 Stability of fluid motion: rectilinear motion of viscous fluid between two parallel plates. *Philos. Mag.* **24**, 188–196.

KERSWELL, R. R. 1994 Tidal excitation of hydromagnetic waves and their damping in the Earth. *J. Fluid Mech.* **274**, 219–241.

KERSWELL, R. R. 2002 Elliptical instability. *Annu. Rev. Fluid Mech.* **34**, 83–113.

KERSWELL, R. R. & MALKUS, W. V. R. 1998 Tidal instability as the source for Io's magnetic signature. *Geophys. Res. Lett.* **25** (5), 603–606.

LACAZE, L., HERREMAN, W., LE BARS, M., LE DIZÈS, S. & LE GAL, P. 2006 Magnetic field induced by elliptical instability in a rotating spheroid. *Geophys. Astrophys. Fluid Dyn.* **100** (4–5), 299–317.

LANDMAN, M. J. & SAFFMAN, P. G. 1987 The three dimensional instability of strained vortices in a viscous fluid. *Phys. Fluids* **30** (8), 2339–2342.

LE BARS, M. & LE DIZÈS, S. 2006 Thermo-elliptical instability in a rotating cylindrical shell. *J. Fluid. Mech.* **563**, 189–198.

LEBOVITZ, N. R. & LIFSCHITZ, A. 1996 Short wavelength instabilities of Riemann ellipsoids. *Phil. Trans. R. Soc. Lond.* A **354**, 927–950.

LEBOVITZ, N. R. & SALDANHA, K. I. 1999 On the weakly nonlinear development of the elliptic instability. *Phys. Fluids* **11**, 3374–3379.

LEBOVITZ, N. R. & ZWEIBEL, E. 2004 Magnetoelliptic instabilities. *Astrophys. J.* **609**, 301–312.

LE DIZÈS, S. 2003 Modal growth and non-modal growth in a stretched shear layer. *Eur. J. Mech.* B **22**, 411–430.

LE DIZÈS, S. & LACAZE, L. 2005 An asymptotic description of vortex Kelvin modes. *J. Fluid Mech.* **542**, 69–96.

LE DIZÈS, S. & LAPORTE, F. 2002 Theoretical predictions for the elliptic instability in a two-vortex flow. *J. Fluid Mech.* **471**, 169.

LE GAL, P., LACAZE, L. & LE DIZÈS, S. 2005 Magnetic field induced by elliptical instability in a rotating tidally-distorted sphere. *J. Phys. Conf. Ser.* **14**, 30–34.

LEWEKE, T. & WILLIAMSON, C. H. K. 1998 Cooperative elliptic instability of a vortex pair. *J. Fluid Mech.* **360**, 85.

MELCHIOR, P. W., CROSSLEY, D. J., DEHANT, V. P. & DUCARME, B. 1988 Have inertial waves been identified from the Earth's core?. In *Structure and Dynamics of the Earth's Deep Interior* (ed. D. E. Smylie & R. Hide), pp. 1–12. American Geophysical Union.

MELCHIOR, P. W. & DUCARME, B. 1986 Detection of inertial gravity oscillations in the Earth's core with a superconducting gravimeter at Brussels. *Phys. Earth Planet. Inter.* **42**, 129.

MEUNIER, P., LE DIZÈS, S. & LEWEKE, T. 2005 Physics of vortex merging. *C. R. Phys.* **6**, 431–450.

MEUNIER, P. & LEWEKE, T. 2001 Three-dimensional instability during vortex merging. *Phys. Fluids* **13**, 2747.

MIYAZAKI, T. 1993 Elliptical instability in a stably stratified rotating fluid. *Phys. Fluids* A **5** (11), 2702–2709.

MIYAZAKI, T. & FUKUMOTO, Y. 1992 Three-dimensional instability of strained vortices in a stably stratified fluid. *Phys. Fluids* A **4** (11), 2515–2522.

MIZERSKI, K. A. & BAJER, K. 2007 The magnetoelliptic instability in the presence of inetrtial forces. In *Advances in Turbulence XI*, Springer Proceedings in Physics, vol. 117, pp. 121–123. Springer. Also in *Proceedings of the 11th EUROMECH European Turbulence Conference*, Porto, Portugal.

MIZERSKI, K. A., BAJER, K. & MOFFATT, H. K. 2009 The α-effect generated by elliptical instability. *J. Fluid Mech.* Submitted.

MOZER, F. S., PHAN, T. D. & BALE, S. D. 2003 The complex structure of the reconnecting magnetopause. *Phys. Plasmas* **10** (6), 2480–2485.

NOIR, J., BRITO, D., ALDRIDGE, K. & CARDIN, P. 2001 Experimental evidence of inertial waves in a precessing spheroidal cavity. *Geophys. Res. Lett.* **19**, 3785–3788.

ORSZAG, S. A. & PATERA, A. T. 1983 Secondary instability of wall-bounded shear flows. *J. Fluid Mech.* **128**, 347–385.

PIERREHUMBERT, R. T. 1986 Universal short-wave instability of two-dimensional eddies in an inviscid fluid. *Phys. Rev. Lett.* **57** (17), 2157–2159.

ROBERTS, P. H. & SOWARD, A. M. 1992 Dynamo theory. *Annu. Rev. Fluid Mech.* **24**, 459–512.

ROTH, M., DE KEYSER, J., DARROUZET, F. & ČADEŽ, V. 2001 Structure and dynamics of the Earth's magnetopause. In *Space Scientific Research in Belgium* vol. 2, part 2, pp. 81, Federal Office for Scientific, Technical and Cultural Affairs (Brussels).

SIPP, D. & JACQUIN, L. 2003 Widnall instabilities in vortex pairs. *Phys. Fluids* **15**, 1861.

SOWARD, A. M. 1991 The Earth's dynamo. *Geophys. Astrophys. Fluid Dyn.* **62**, 191–209.

SUESS, S. T. 1970 Some effects of gravitational tides on a model Earth's core. *J. Geophys. Res.* **75**, 6650–6661.

THESS, A. & ZIKANOV, O. 2007 Transition from two-dimensional to three-dimensional magneto-hydrodynamic turbulence. *J. Fluid Mech.* **579**, 383–412.

TILGNER, A. 2005 Precession driven dynamos. *Phys. Fluids* **17**, 034104.

VANYO, J., WILDE, P., CARDIN, P. & OLSON, P. 1995 Experiments on precessing flows in the Earth's liquid core. *Geophys. J. Intl* **121**, 136–142.

WALEFFE, F. 1990 On the three-dimensional instability of strained vortices. *Phys. Fluids* A **2** (1), 76–80.

WIENBRUCH, U. & SPOHN, T. 1995 A self-sustained magnetic field on Io?. *Planet. Space. Sci.* **43**, 1045–1057.